drones

MDPI

Article

High-Order Disturbance Observer-Based Fuzzy Fixed-Time Safe Tracking Control for Uncertain Unmanned Helicopter with Partial State Constraints and Multisource Disturbances

Ruonan Ren [1,2], Zhikai Wang [2,3], Haoxiang Ma [2,3], Baofeng Ji [1,2] and Fazhan Tao [1,2,*]

[1] Longmen Laboratory, Luoyang 471023, China; 220320040426@stu.haust.edu.cn (R.R.); fengbaoji@126.com (B.J.)
[2] College of Information Engineering, Henan University of Science and Technology, Luoyang 471023, China; zhikaiwang01@163.com (Z.W.); hxma@haust.edu.cn (H.M.)
[3] Henan Key Laboratory of Robot and Intelligent System, Henan University of Science and Technology, Luoyang 471023, China
* Correspondence: taofazhan@haust.edu.cn

Abstract: In the real-world operation of unmanned helicopters, various state constraints, system uncertainties and multisource disturbances pose considerable risks to their safe fight. This paper focuses on anti-disturbance adaptive safety fixed-time control design for the uncertain unmanned helicopter subject to partial state constraints and multiple disturbances. Firstly, a developed safety protection algorithm is integrated with the fixed-time stability theory, which assures the tracking performance and guarantees that the partial states are always constrained within the time-varying safe range. Then, the compensation mechanism is developed to weaken the adverse impact induced by the filter errors. Simultaneously, the influence of the multisource disturbances on the system stability are weakened through the Itô differential equation and high-order disturbance observer. Further, the fuzzy logic system is constructed to approximate the system uncertainties caused by the sensor measurement errors and complex aerodynamic characteristics. Stability analysis proves that the controlled unmanned helicopter is semi-globally fixed-time stable in probability, and the state errors converge to a desired region of the origin. Finally, simulations are provided to illustrate the performance of the proposed scheme.

Keywords: unmanned helicopter; safety protection algorithm; fuzzy logic system; fixed-time stability theory; command filter; high-order disturbance observer

Citation: Ren, R.; Wang, Z.; Ma, H.; Ji, B.; Tao, F. High-Order Disturbance Observer-Based Fuzzy Fixed-Time Safe Tracking Control for Uncertain Unmanned Helicopter with Partial State Constraints and Multisource Disturbances. *Drones* **2024**, *8*, 679. https://doi.org/10.3390/drones8110679

Academic Editor: Abdessattar Abdelkefi

Received: 24 August 2024
Revised: 12 November 2024
Accepted: 15 November 2024
Published: 18 November 2024

1. Introduction

Due to their simple operation and low price, unmanned autonomous helicopters (UAHs) have been widely used in many fields in recent decades, such as the military [1], agriculture [2] and logistics [3]. With the increasing attention, the shortcomings of unmanned helicopters, such as uncertainties, multiple disturbances and high nonlinearity, their security controls have received a lot of attention [4–6]. In addition, UAHs usually use a variety of sensors, such as Global Positioning System (GPS), Inertial Measurement Unit (IMU), air pressure sensors, etc., so they have strong coupling characteristics. For example, changes in sensor data will direcly affect changes in various states of the UAHs. In addition, there is coupling between the communication system and the data processing unit, the load and power system, and the thermal management system and the power system. To this end, many nonlinear control methods have been proposed. In [7], the authors employed the feedback linearization technique to a laboratory helicopter system, which reduces the conservativeness of the robust compensator design. Based on the adaptive backstepping technique, the authors developed the output-feedback baseline controller for helicopters in [8], where the adaptive control technique improves the shock absorption capability of

the controller. Subsequently, because the backstepping technique can through repeated iteration and adjustment make the controller have a more superior performance, it is employed by the majority of scholars for unmanned helicopter control, such as in [5,9–11]. In order to reduce the controller computational burden in the backstepping technique due to iteration, the dynamic surface control (DSC) scheme was adopted [12]. However, if the new filtering error obtained by the DSC method cannot be compensated, the system performance will be reduced. Fortunately, the command-filtered backstepping control (CFBC) scheme can solve the problem above by using a compensating signal to compensate for the filtering error [13]. Since then, the CFBC and many advanced control methods are used in unmanned helicopter systems [14,15]; for example, in [14], the authors employed the CFBC-based fault-tolerant control strategy for drone interceptors. It can be observed that the works above can only control the unmanned helicopter under ideal conditions. However, UAHs have always suffered with system uncertainties and disturbances when flying because of their special rigid structure and complex working environments; if these situations are not considered when designing the controller, the control performance will be reduced or even ineffective.

Given that the nonlinear functions can be approximated well by the fuzzy logic system (FLS), the FLS control scheme has been applied for uncertain systems [16–21]. In [17], a proportional–integral–derivative (PID)-based adaptive fuzzy control algorithm was developed for a UAH with system uncertainties, and the simulation shows that the proposed controller method has a better effect on the system uncertainties. In [19], based on Takagi–Sugeno FLS, an event-triggering controller is designed for the system with DoS attack. The authors in [20] proposed a fuzzy wavelet neural adaptive control scheme for a quadrotor UAV; the simulation represented the control performance of the proposed control approach. The authors in [21] applied FLS to an unmanned aerial vehicle formation system to solve the system uncertainties existing in the system. In addition to the system uncertainties caused by complex dynamic models, the external disturbances often occur during unmanned helicopter operations [22]. The authors estimate the maximum value of the disturbance and convert it into a constant using inequality to eliminate it in [23]. Then, in order to eliminate the effect of real-time disturbances on the system better, the corresponding disturbance observer was employed [24–26]. In [24], to estimate the unknown disturbances, the authors investigated the disturbance observer (DO). However, the random disturbances in the unmanned helicopter system, caused by internal noise and sensor measurement errors, are not mentioned. Because of its randomness, disorder and rapid change on a small scale, the general disturbance observer can not deal with random disturbances well. To this end, the authors in [27] developed the extended state observer to approximate the random disturbances of the second-order stochastic multiagent systems. Furthermore, Itô differential equation is composed of partial differential equations with random terms, so it can deal with random disturbances contained in the system [28,29]. In [29], the authors suggested the Itô differential equation to solve the random disturbances for a class of nonlinear stochastic Poisson signal systems.

It is worth noting that the works above solve the stability problem of an unmanned helicopter when there is system uncertainty, external disturbances and random disturbances. However, due to the complex working environments, the state constraint of UAHs is also a topic worth studying. For the problem of dealing with constraints, scholars have proposed many methods. For example, the model predictive control (MPC) [30,31], reference governor approach [32,33], barrier Lyapunov function (BLF) [34,35], the prescribed performance function (PPC) [36–38] and so on. In [30], based on the Hammerstein model, the authors developed the MPC method for unmanned aerial vehicles, which allows the unmanned autonomous vehicles (UAVs) to track the target accurately. The authors in [33] utilized the reference governor approach for the affine systems. The BLF was utilized in [34] to constrain the output of the UAH. The PPC technique was employed in [38] for the 3-degree-of-freedom helicopters, which can constrain the error within the safe range. However, the MPC and reference governor approaches rely on system models,

and unmanned helicopter models are highly complex, making it difficult to create accurate mathematical models. BLF and PPC constrain the state by constraining the state error, which depends on "feasibility conditions", but the feasibility conditions are often difficult to obtain. The proposal of the safety protection algorithm (SPA) solves the problem above [39], which can obtain real-time boundary constraints through airborne sensors, and combined with a preset expectation signals, generate a new safety expectation signals. However, the methods above all use the general asymptotic stability method, the system may take a long time to reach stability, and UAHs have high requirements for speed and accuracy.

The fixed-time stability theory can make the system settling time independent of the initial state of the system [40,41], so it has been studied by most scholars. In the last decade, the fixed-time stability theory and other mainstream methods have been combined for use in various systems. In [42], the fixed-time stability theory was combined with the adaptive control method for a class nonlinear systems. The authors in [43] combined the fixed-time theory and DO to form a fixed-time disturbance observer, which guarantees that all states and disturbance converge to the desired ranges in fixed time. In [44], the sliding mode control-based fixed-time controller was developed, which improves the resource utilization, robustness and response speed of the system. In [45], inspired by the Itô Lemma, the authors developed a novel fixed-time stability criterion for the stochastic pure-feedback system.

Inspired by the works above, this paper investigates the adaptive safety fixed-time tracking control scheme with a high-order disturbance observer (HODO) for the uncertain unmanned helicopter suffering multisource disturbances and external disturbances. The following are the chief contributions of this paper:

- In order to keep partial states of the unmanned helicopter system within the time-varying safety boundary, the desired safety signals are constructed by SPA, which avoids the disadvantages of traditional BLF and PPC, indirectly constrains the state through constraint state errors and eliminates the assumption of feasibility conditions. In addition, second-order DSC is used to make the desired safety signals continuously differentiable.
- Compared with asymptotic stability control and finite-time stability theory, the fixed-time stability theory ensures that the controlled unmanned helicopter system is semi-globally fixed-time stable in probability, and the convergence time of the system only depends on the devised parameters. Moreover, the compensation mechanism is employed to improve the tracking performance and robustness of the controller system.
- Unlike from the existing DO and FTDO in [43], the developed HODO provides an unbiased estimate of the reciprocal of the external disturbances, which realizes the precise control and compensation of the external disturbances. In addition, FLS and the Itô differential equation are employed to handle the system uncertainties and random disturbances.

The structure of this paper is as follows: Section 2 outlines the necessary preparations. Section 3 presents the control strategy. Section 4 discusses the primary stability analysis. Section 5 shows the simulation results, and Section 6 concludes the paper.

2. Necessary Preparation

In this section, the dynamic model of a UAH is provided, along with some of the necessary problem formulation, Lemmas and Assumptions.

2.1. Modeling of the UAH

In order to make the research object more clear, the schematic diagram of the UAH system is provided in Figure 1.

According to the aerodynamics and flight dynamics, the dynamics of 6-DOF UAH can be expressed as [5].

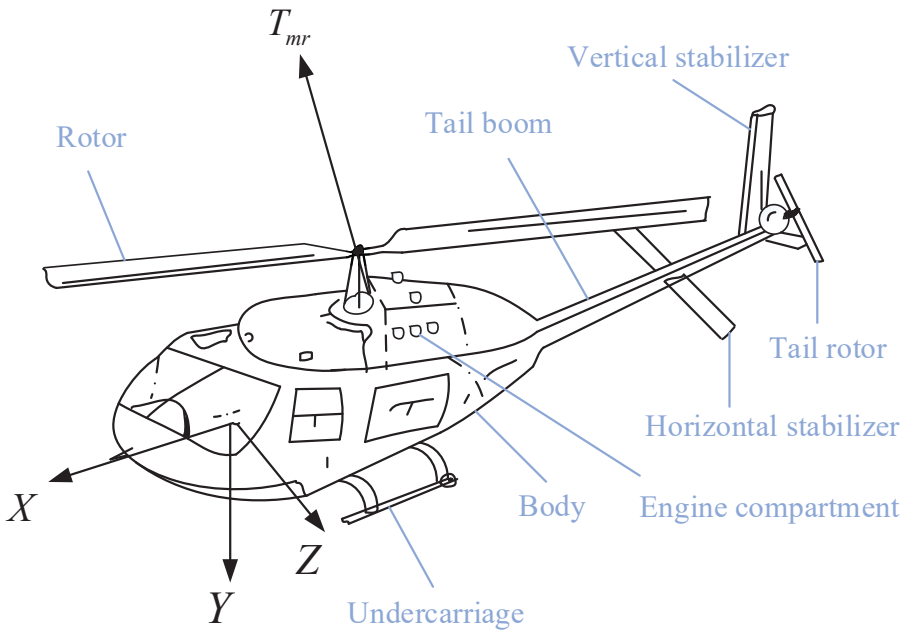

Figure 1. Schematic diagram of the UAH system.

$$\begin{cases} dP = Vdt \\ dV = (\Sigma_1/m + G + \Delta f_V + d_1)dt + G_V d\omega \\ d\Omega = H\mu dt \\ d\mu = (-J^{-1}\mu \times J\mu + \Delta f_\mu + J^{-1}\Sigma_2 + d_2)dt + G_\mu d\omega, \end{cases} \tag{1}$$

where $P = [X, Y, Z]^{\mathrm{T}}, V = [u, v, w]^{\mathrm{T}}, \Omega = [\phi, \theta, \psi]^{\mathrm{T}}$ and $\mu = [p, q, r]^{\mathrm{T}}$ denote the position vector, velocity vector, attitude angle vector and angular velocity vector of the unmanned helicopter, respectively. m represents the mass of the unmanned helicopter. $\Sigma_1 = RF_V$ with $F_V = [0, 0, -T_{mr}]^{\mathrm{T}}, \Sigma_2 = [\Sigma_X, \Sigma_Y, \Sigma_Z]^{\mathrm{T}}$. $G = [0, 0, g]^{\mathrm{T}}$ with g is the gravity acceleration, $T_{mr}, \Sigma_X, \Sigma_Y, \Sigma_Z$ stands for the inputs. $R \in \Re^{3\times3}$ represents the coordinate transformation matrix [5] and $H \in \Re^{3\times3}$ stands for the attitude kinematic matrix [11]. $J = \mathrm{diag}\{J_{xx}, J_{yy}, J_{zz}\}$ is the inertia matrix. $\Delta f_V \in \Re^3, \Delta f_\mu \in \Re^3$ are the system uncertainties, $d_1 \in \Re^3$ and $d_2 \in \Re^3$ represent the external disturbances. G_V, G_μ are known functions.

In order to better demonstrate the dynamic characteristics of an unmanned helicopter system, (1) can be divided into the position loop

$$\begin{cases} dP = Vdt \\ dV = (\Sigma_1/m + G + \Delta f_V + d_1)dt + G_V d\omega, \end{cases} \tag{2}$$

and the attitude loop

$$\begin{cases} d\Omega = H\mu dt \\ d\mu = (-F_\mu + \Delta f_\mu + J^{-1}\Sigma_2 + d_2)dt + G_\mu d\omega, \end{cases} \tag{3}$$

where $F_\mu = J\mu \times J\mu$.

2.2. Problem Formulation

The stochastic nonlinear system can be expressed as

$$\dot{\hbar}(t) = F(\hbar)dt + G^{\mathrm{T}}d\omega, \hbar(0) = \hbar_0, \tag{4}$$

where $\hbar \in \Re^n$, $F(\hbar) : \Re^n \to \Re^n$ and $G(\hbar) : \Re^n \to \Re^{n\times m}$ are the state and smooth functions. ω is r-dimension Brownian motion. For system (1), it has $W(\hbar, t) \in C^{2,1}$, and the differential operator L is defined as

$$\mathcal{L}W = \frac{\partial W}{\partial t} + \frac{\partial W}{\partial \hbar} f + \frac{1}{2}\mathrm{tr}\left\{G^{\mathrm{T}} \frac{\partial^2 W}{\partial^2 \hbar} G\right\}. \tag{5}$$

Lemma 1 ([42]). *For any variables $\Im_1, \Im_2 \in \Re, \Im_3 > 0, \Im_4 > 0, \Im_5 > 0$, one has*

$$|\Im_1|^{\Im_3}|\Im_2|^{\Im_4} \leq \frac{\Im_3}{\Im_3 + \Im_4}\Im_5|\Im_1|^{\Im_3+\Im_4} + \frac{\Im_4}{\Im_3 + \Im_4}\Im_5 - \frac{\Im_3}{\Im_4}|\Im_2|^{\Im_3+\Im_4}. \tag{6}$$

Lemma 2 ([44]). *Consider the FLS as follows:*

$$\begin{gathered} \textit{Rule: If } \hbar_1 \textit{ is } \aleph_1^i \textit{ nd } \hbar_2 \textit{ is } \aleph_1^i \cdots \hbar_n \textit{ is } \aleph_n^i \\ \textit{Then } y \textit{ is } \wp^i, i = 1, 2, \cdots, k \end{gathered}$$

where $\hbar = [\hbar_1, \hbar_2, \cdots, \hbar_n]^{\mathrm{T}}$ and y represent the input and output of the FLS, respectively. $\aleph_j^i$ and $\wp^i (i = 1, 2, \cdots, k, j = 1, 2, \cdots, n)$ denote the fuzzy sets corresponding to fuzzy membership function $a_{\aleph_j^i}$ and $a_{\wp^i}$, respectively. k is the number of rules. Through a series of operations, FLS can be written as

$$y = \frac{\sum_{i=1}^{k} \bar{y}_i \prod_{j=1}^{n} a_{\aleph_j^i}(\hbar_j)}{\sum_{i=1}^{k}\left[\prod_{j=1}^{n} a_{\wp^i}(\hbar_j)\right]} \tag{7}$$

where $\bar{y}_i = \max\limits_{y\in\Re} a_{\wp^i}(y)$.

The fuzzy basis function is defined as

$$k_i = \frac{\prod_{j=1}^{m} a_{\aleph_j^i}(\hbar_j)}{\sum_{i=1}^{k}\left[\prod_{j=1}^{n} a_{\wp^i}(\hbar_j)\right]}, i = 1, 2, \cdots, k \tag{8}$$

Then the FLS can be represented as

$$f(\hbar) = \hat{\omega}^{\mathrm{T}} \Xi(\hbar) \tag{9}$$

where $\hat{\omega} = [\bar{y}_1, \bar{y}_2, \cdots, \bar{y}_k]^{\mathrm{T}}$ and $\Xi_1(\hbar) = [\Xi_2(\hbar), \cdots, \Xi_k(\hbar)]^{\mathrm{T}}$ are the adjustable parameter vector and fuzzy basis function vector, respectively.

Further, Lemma 2 can be redefined as follows:

If there is a known function $f(\hbar)$ defined on a compact Δ, then FLS can approximate it as follows:

$$f(\hbar) = \varpi^{\mathrm{T}} \Xi(\hbar) + \sigma^*, \tag{10}$$

where σ^* is the approximate error.

Lemma 3 ([42]). *For (1), there exist some constants $K > 0, 0 < \jmath < 1, L > 0, \ell > 1, 0 < M < \infty, 0 < \rho < 1$, such that*

$$\dot{W}(\hbar) \leq -KW^{\jmath}(\hbar) - LW^{\ell}(\hbar) + M, \tag{11}$$

then, (4) means a semi-globally fixed-time state in probability. The settling time is estimated as

$$T \leq T_{\max} : \frac{1}{K\rho(1-\jmath)} + \frac{1}{L\rho(\ell-1)}. \tag{12}$$

Lemma 4 ([43]). *There exist some constants satisfying $0 < \jmath < 1, \ell > 1, m_i \in \Re$, then one can obtain $(m_1 + m_2 + \cdots + m_n)^{\jmath} \leq m_1^{\jmath} + m_2^{\jmath} + \jmath + m_n^{\jmath}$, $n^{1-\ell}(m_1 + m_2 + \cdots + m_n)^{\ell} \leq m_1^{\ell} + m_2^{\ell} + \cdots + m_n^{\ell}$.*

Assumption 1 ([5]). *The external disturbances d_1, d_2 and $\dot{d}_1, \dot{d}_2$ are bounded.*

Assumption 2 ([5]). *The desired signals and their 1- and 2-order derivatives are bounded.*

Assumption 3 ([5]). *All states of the UAH system (1) are measurable.*

3. Controller Design

In this section, the safety trajectory vectors $P_r = [X_r, Y_r, Z_r]^{\mathrm{T}}, \Omega_r = [\phi_r, \theta_r, \psi_r]^{\mathrm{T}}$ are designed through the SPA. The adaptive safety fixed-time anti-disturbance controller is designed with the backstepping technique. The control diagram is provided in Figure 2, and the variables contained therein will be introduced later.

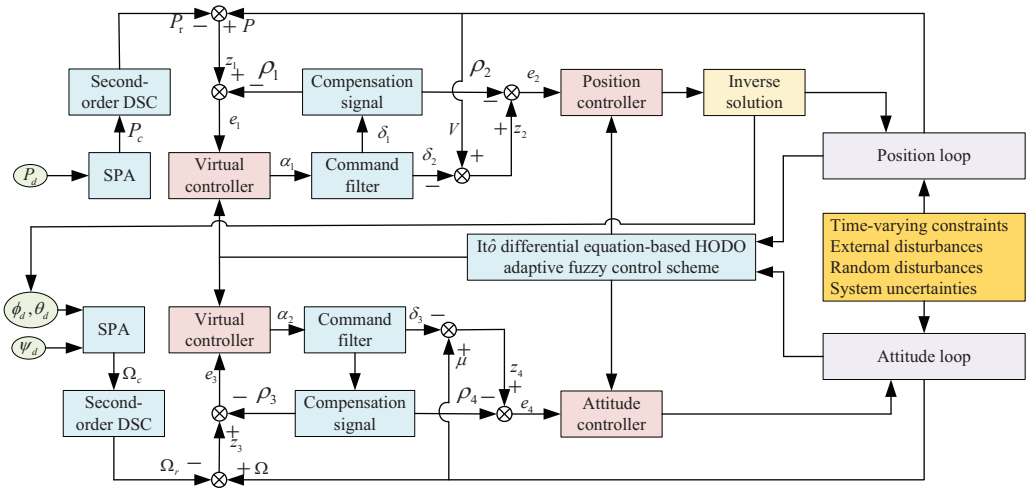

Figure 2. Control diagram of this paper.

3.1. Desired Safety Trajectory Generation

In order to obtain the expected safety signal, based on the SPA, take the X-axis, and for example, define X_{up} and X_{low} as the upper and lower bounds of the smooth safe boundaries, then the generation steps of X_r are as follows:

Case I: $X_d \geq X_{up} - \varepsilon_X$:

$$X_c^{(r)} = X_{up}^{(r)} - \varepsilon_X^{(r)},$$

Case II: $X_d \leq X_{low} + \varepsilon_X$:

$$X_c^{(r)} = X_{low}^{(r)} + \varepsilon_X^{(r)},$$

Case III: $X_{low}^{(r)} + \varepsilon_X^{(r)} \leq X_d \leq X_{up}^{(r)} - \varepsilon_X^{(r)}$

$$X_c^{(r)} = X_d^{(r)},$$

where $r = 1, 2$. $\varepsilon_X = h_X(X_{up} - X_{low})$ represents the time-varying margin with $h \in (0, 0.5)$.

Therefore, $Y_c^{(r)}, Z_c^{(r)}$ and $\phi_c^{(r)}, \theta_c^{(r)}, \psi_c^{(r)}$ can be obtained by the same process.

Remark 1. *For the common BLF*

$$W = \log \frac{k^2}{k^2 - z^2} \tag{13}$$

where $z = x - x_d$ with x and x_d are the state and desired signal, k is the constraint of z. This method of constraint converts the original state constraint into new bounds of the tracking error.

This approach has a disadvantage; that is, when the difference between the error and the constraint condition is small, a larger control force is needed to adjust the performance of system. The biggest difference between the SPA and BLF constraints used in this article is that SPA can evaluate the expected signal in advance and then compare it with the original expected signal to generate a new expected safety signal, and use the constrained desired safety trajectory to design the controller. Therefore, there is no need to constrain the state error, and the input cannot be too large beyond the safe range of the system. In addition, the time-varying safety margin ε is considered in this paper, which further improves the safety performance of the system.

However, the generated segmented safety expectation signal cannot be directly differentiated. In order to be able to use the backstepping technique, a second-order DSC is used to convert the segmented ζ_c into a continuously reversible ζ_r. Define $\delta_\zeta = [\zeta_r^{\mathrm{T}}, r_\zeta^{\mathrm{T}}]^{\mathrm{T}}$ with ζ_r and r_ζ as the estimates of ζ_c and $\dot{\zeta}_c$, respectively. Then, the second-order DSC can be represented as

$$\dot{\delta}_\zeta = A_0\delta_\zeta + B_0\zeta_c, \tag{14}$$

where ζ_c and ζ_r are the input and output of the second-order DSC, respectively.

$$A_0 = \begin{bmatrix} -\sigma_1 & 0 \\ -\sigma_2 & 0 \end{bmatrix}, \qquad B_0 = \begin{bmatrix} -\sigma_1 \\ -\sigma_2 \end{bmatrix},$$

Then, a theorem is given as follows:

Theorem 1. *Let ζ_c pass through the second-order DSC (14), then the generated trajectory ζ_r is smooth and differentiable.*

Proof. Defining $\widetilde{\delta}_\zeta = [\widetilde{\zeta}_r, \widetilde{r}]^{\mathrm{T}}$ with $\widetilde{\zeta}_r = \zeta_r - \zeta_c, \widetilde{r} = r - \dot{\zeta}_c$, one has

$$\dot{\widetilde{\delta}}_\zeta = A_\zeta\widetilde{\delta}_\zeta + N_\zeta, \tag{15}$$

where $N_\zeta = [0_3^{\mathrm{T}}, \ddot{\zeta}_c]$.

Select the Lyapunov as

$$W_\varsigma = \widetilde{\delta}_\zeta^{\mathrm{T}} P_\zeta \widetilde{\delta}_\zeta. \tag{16}$$

Taking the derivative of (16), one can obtain

$$\begin{aligned} \dot{W}_\varsigma =& \widetilde{\delta}_\zeta^{\mathrm{T}}(A_\zeta^{\mathrm{T}}P_\zeta + P_\zeta A_\zeta)\widetilde{\delta}_\zeta + 2\widetilde{\delta}_\zeta^{\mathrm{T}}P_\zeta N_\zeta \\ =& -\widetilde{\delta}_\zeta^{\mathrm{T}}Q_0\widetilde{\delta}_\zeta + 2\widetilde{\delta}_\zeta^{\mathrm{T}}P_\zeta N_\zeta. \end{aligned} \tag{17}$$

Invoking **Lemma 1**, one has

$$2\widetilde{\delta}_\zeta^{\mathrm{T}}P_\zeta N_\zeta \le \widetilde{\delta}_\zeta^{\mathrm{T}}P_\zeta^2\widetilde{\delta}_\zeta + ||N_\zeta||^2. \tag{18}$$

Substituting (18) into (17) yields

$$\begin{aligned} \dot{W}_\varsigma \le& -\widetilde{\delta}_\zeta^{\mathrm{T}}(Q_\zeta - P_\zeta^2)\widetilde{\delta}_\zeta + 2\widetilde{\delta}_\zeta^{\mathrm{T}}P_\zeta N_\zeta \\ =& -a_\zeta\widetilde{\delta}_\zeta^{\mathrm{T}}P_\zeta\widetilde{\delta}_\zeta + M_\zeta, \end{aligned} \tag{19}$$

where $a_\zeta = \lambda_{\min}(Q_\zeta - P_\zeta^2)/\lambda_{\min}(P_\zeta), M_\zeta = ||N_\zeta||$

Integration of (19) yields

$$0 \le W_\zeta \le \frac{M_\zeta}{a_\zeta} + \left[W_\zeta(0) - \frac{M_\zeta}{a_\zeta}\right]e^{-a_\zeta t} \le W_\zeta(0) + \frac{M_\zeta}{a_\zeta}. \tag{20}$$

From (16), one has

$$|\Gamma_r - \Gamma_c| \leq ||\zeta_r|| \leq \sqrt{2(W_\Gamma(0) + M_\Gamma/a_\Gamma)}, \tag{21}$$

where $\Gamma \in \{X, Y, Z, \phi, \theta, \psi\}$.

It can be shown that by selecting suitable upper and lower bounds, designing parameters $a_\Gamma, \varepsilon_\Gamma$ and passing through the second-order DSC, the real-time constrained desired signals can be obtained, where $a_\Gamma, \varepsilon_\Gamma$ satisfy the following conditions:

$$\begin{cases} a_\Gamma > 0 \\ \varepsilon_\Gamma > \sqrt{2(W_\zeta(0) + M_\Omega/a_\Gamma)}. \end{cases}$$

This concludes the proof. □

3.2. Design of the Command Filter

The tracking errors are provided as

$$z_1 = P - \delta_1, \tag{22}$$
$$z_2 = V - \delta_2, \tag{23}$$
$$z_3 = \Omega - \delta_3, \tag{24}$$
$$z_4 = \mu - \delta_4, \tag{25}$$

where $\delta_1, \delta_2, \delta_3$ and δ_4 stand for the outputs of command filter, which are constructed as

$$\begin{cases} \dot{\delta}_1 = \Gamma_1 \eta_1 \\ \dot{\eta}_1 = -2\nu_1\Gamma_1\eta_1 - \Gamma_1(\delta_1 - P_r), \end{cases} \tag{26}$$

$$\begin{cases} \dot{\delta}_2 = \Gamma_2 \eta_2 \\ \dot{\eta}_2 = -2\nu_2\Gamma_2\eta_2 - \Gamma_2(\delta_2 - \alpha_1), \end{cases} \tag{27}$$

$$\begin{cases} \dot{\delta}_3 = \Gamma_3 \eta_3 \\ \dot{\eta}_3 = -2\nu_3\Gamma_3\eta_3 - \Gamma_3(\delta_3 - V_r), \end{cases} \tag{28}$$

$$\begin{cases} \dot{\delta}_4 = \Gamma_4 \eta_4 \\ \dot{\eta}_4 = -2\nu_4\Gamma_4\eta_4 - \Gamma_4(\delta_4 - \alpha_2), \end{cases} \tag{29}$$

where $\eta_i, (i = 1, 2, 3, 4)$ are auxiliary variables of the command filter, and α_1, α_2 are the virtual controller to be designed later. $\Gamma_i \in \Re^{3\times3}, (i = 1, 2, 3, 4)$ stands for the design matrix, and $\nu_i \in (0, 1], (i = 1, 2, 3, 4)$ are design parameters. In addition, $\delta_1(0) = P_r(0), \delta_2(0) = \alpha_2(0), \delta_3(0) = V_r(0), \delta_4(0) = \alpha_4(0)$ $\eta_i(0) = 0_3$.

To eliminate the effect of filtering errors, the compensations mechanisms are defined as

$$e_1 = z_1 - \rho_1, \tag{30}$$
$$e_2 = z_2 - \rho_2, \tag{31}$$
$$e_3 = z_3 - \rho_3, \tag{32}$$
$$e_4 = z_4 - \rho_4, \tag{33}$$

where $\rho_1, \rho_2, \rho_3, \rho_4$ are compensation functions and designed as follows:

$$\begin{cases} \dot{\rho}_1 = \rho_2 + \delta_2 - \alpha_1 - k_{\rho_1}\rho_1 \\ \dot{\rho}_2 = -k_{\rho_2}\rho_2 \\ \dot{\rho}_3 = H\rho_4 + H\delta_4 - \alpha_2 - k_{\rho_3}\rho_3 \\ \dot{\rho}_4 = -k_{\rho_4}\rho_4, \end{cases} \tag{34}$$

where $k_{\rho 1}, k_{\rho 2}, k_{\rho 3}, k_{\rho 4}$ are positive design parameters.

3.3. HODO-Based Adaptive Safety Fixed-Time Tracking Controller Design

To handle the impact of Δf_V and Δf_μ on the system, the FLS is utilized, as follows:

$$\Lambda_1 \Delta f_V = \varpi_1^{\mathrm{T}} \Xi_1 + \sigma_1^*, \tag{35}$$

and

$$\Lambda_2 \Delta f_\omega = \varpi_2^{\mathrm{T}} \Xi_2 + \sigma_2^*, \tag{36}$$

where $\Lambda_i = \Lambda_i^{\mathrm{T}} \in \Re^{3\times 3}, (i = 1, 2)$ are design matrices, and σ_1^*, σ_2^* are estimate errors.

Then (2) and (3) can be rewritten as

$$\begin{cases} dP = Vdt \\ dV = (\Sigma_1/m + G + \Lambda_1^{-1}\varpi_1^{\mathrm{T}}\Xi_1 + D_1)dt + G_V d\omega, \end{cases} \tag{37}$$

and

$$\begin{cases} d\Omega = H\mu dt \\ d\mu = (-F_\mu + \Lambda_2^{-1}\varpi_2^{\mathrm{T}}\Xi_2 + D_2 + J^{-1}\Sigma_2)dt + G_\mu d\omega, \end{cases} \tag{38}$$

where $D_i = d_i + \Lambda_i^{\mathrm{T}}\sigma_i^*, (i = 1, 2)$

Step 1: By invoking (22), (23), (26), (30), (31) and (34), one has

$$de_1 = (e_2 + k_{\rho_1}\rho_1 - \dot{\delta}_1 + \alpha_1)dt. \tag{39}$$

Select the Lyapunov function as

$$W_1 = \frac{1}{4}(e_1^{\mathrm{T}} e_1)^2. \tag{40}$$

Take the derivative of V_1, and utilizing (39) produces

$$\mathcal{L}W_1 = e_1^{\mathrm{T}} A_1 (e_2 + k_{\rho_1}\rho_1 - \dot{\delta}_1 + \alpha_1), \tag{41}$$

where $A_1 = \mathrm{diag}\{e_{11}^2; e_{12}^2; e_{13}^2\}$.

Invoking **Lemma 1**, one can obtain

$$e_1^{\mathrm{T}} A_1 e_2 \le \frac{3}{4} e_1^{\mathrm{T}} A_1 e_1 + \frac{1}{4} e_2^{\mathrm{T}} A_2 e_2, \tag{42}$$

where $A_2 = \mathrm{diag}\{e_{21}^2; e_{22}^2; e_{23}^2\}$.

Substituting (39) into (41) yields

$$\mathcal{L}W_1 \le e_1^{\mathrm{T}} A_1 (k_{\rho_1}\rho_1 - \dot{\delta}_1 + \frac{3}{4} e_1 + \alpha_1) + \frac{1}{4} e_2^{\mathrm{T}} A_2 e_2, \tag{43}$$

Choose the virtual controller as

$$\begin{aligned}\alpha_1 = &-h_{11}A_1^{2J-1}e_1 - h_{12}A_1^{2\ell-1}e_1 + \dot{\delta}_1\\ &-\frac{1}{2}A_1\Lambda_1^{-2}e_1 - \frac{3}{4}e_1 - k_{\rho_1}\rho_1,\end{aligned} \tag{44}$$

where $h_{i1} \in \Re^{3\times 3} \succ 0, h_{i2} \in \Re^{3\times 3} \succ 0, (i = 1, 2, 3, 4)$ are design matrices.

Substituting (46) into (44), one yields

$$\begin{aligned}\mathcal{L}W_1 = &-e_1^{\mathrm{T}}h_{11}A_1^{2J-1}e_1 - e_1^{\mathrm{T}}h_{12}A_1^{2\ell-1}e_1\\ &+\frac{1}{4}e_2^{\mathrm{T}}A_2e_2 + \frac{1}{2}\sigma_1^2.\end{aligned} \tag{45}$$

Step 2: Taking the derivative of (31) yields

$$de_2 = (\Sigma_1/m + G + \Lambda_1^{-1}\omega_1^{\mathrm{T}}\Xi_1 + D_1 - \dot{\delta}_2 + k_{\rho_2}\rho_2)dt + G_V d\omega. \tag{46}$$

In order to approximate the compound disturbance D_1, the HODO is constructed as

$$\begin{cases}\hat{D}_1 = \eta_{11} + k_{11}X_1,\\ \dot{\eta}_{11} = -k_{11}\left(\frac{\Sigma_1}{m} + G + \hat{D}_1 + \Lambda_1^{-1}\omega_1^{\mathrm{T}}\Xi_1\right) + \dot{\hat{D}}_1,\\ \dot{\hat{D}}_1 = \eta_{12} + k_{12}X_1,\\ \dot{\eta}_{12} = -k_{12}\left(\frac{\Sigma_1}{m} + G + \hat{D}_1 + \Lambda_1^{-1}\omega_1^{\mathrm{T}}\Xi_1\right) + \ddot{\hat{D}}_1,\\ \cdots\\ \hat{D}_1^{(r-1)} = \eta_{1r} + k_{1r}X_1,\\ \dot{\eta}_{1r} = -k_{1r}\left(\frac{\Sigma_1}{m} + G + \hat{D}_1 + \Lambda_1^{-1}\omega_1^{\mathrm{T}}\Xi_1\right),\end{cases} \tag{47}$$

where $\hat{D}_1 \in \Re^3, \dot{\hat{D}}_1 \in \Re^3, \ldots, \hat{D}_1^{(r-1)} \in \Re^3$ are the estimates of $D_1, \dot{D}_1, \ldots, D_1^{(r-1)}$. $\eta_{1r} \in \Re^3$ are auxiliary variables, $k_{1r} \in \Re^{3\times 3} \succ 0$ are design matrices and $\dot{X}_1 = \Sigma_1/m + G + \Lambda_1^{-1}\omega_1^{\mathrm{T}}\Xi_1 + D_1$.

Defining $\widetilde{\hat{D}}_1 = [\tilde{D}_1^{\mathrm{T}}, \dot{\tilde{D}}_1^{\mathrm{T}}, \ldots, (\tilde{D}_1^{r-1})^{\mathrm{T}}]^{\mathrm{T}}$ with $\tilde{D}_1^s = D_1^s - \hat{D}_1^s, (s = 1, 2, \cdots, r-1)$, then one can obtain

$$\dot{\widetilde{\hat{D}}}_1 = K_1\widetilde{\hat{D}}_1 + D_1^* + K_1^*\Phi_1^{\mathrm{T}}\Xi_1^*, \tag{48}$$

where $K_1^* = \mathrm{diag}\{k_{11}; k_{12}; \cdots, k_{1r}\}$,

$$D_1^* = \begin{bmatrix}0\\ 0\\ \vdots\\ D_1^r\end{bmatrix}, \qquad K_1 = \begin{bmatrix}k_{11} & I_3 & \cdots & 0 & 0\\ k_{12} & 0_3 & I_3 & \cdots & 0_3\\ \vdots & \vdots & \vdots & \cdots & \vdots\\ k_{1r} & 0_3 & 0_3 & \cdots & 0\end{bmatrix},$$

and K_1 is a Hurwitz matrix. Thus, by choosing approximate design positive definite matrices $P_1 = P_1^{\mathrm{T}} \in \Re^{3r\times 3r}$, one can obtain

$$K_1^{\mathrm{T}}P_1 + P_1K_1 = -Q_1, \tag{49}$$

where $Q_1 = Q_1^{\mathrm{T}} \in \Re^{3r\times 3r}$.

The Lyapunov function is constructed as

$$W_2 = \frac{1}{4}(e_2^{\mathrm{T}}e_2)^2 + \widetilde{D}_1^{\mathrm{T}}P_1\widetilde{D}_1 + \frac{1}{2\gamma_1}\mathrm{tr}(\widetilde{\omega}_1\widetilde{\omega}_1), \tag{50}$$

where $\gamma_i > 0, (i = 1, 2)$ are design constants and $\widetilde{\omega}_i = \omega_i - \hat{\omega}_i$ and $\hat{\omega}_i$ are the estimate errors and estimates of $\omega_i, (i = 1, 2)$.

Taking the derivative of W_2 produces

$$\begin{aligned}\mathcal{L}W_2 \leq & e_2^{\mathrm{T}}A_2(\Sigma_1/m + G + \Lambda_1^{-1}\omega_1^{\mathrm{T}}\Xi_1 + D_1 - \dot{\delta}_2 + k_{\rho_2}\rho_2) \\ & + \frac{3}{2}e_2^{\mathrm{T}}e_2G_V^{\mathrm{T}}G_V - \frac{1}{\gamma_1}\mathrm{tr}(\widetilde{\omega}_1^{\mathrm{T}}\dot{\hat{\omega}}_1) + 2\widetilde{\widetilde{D}}_1^{\mathrm{T}}P_1D_1^* \\ & + \widetilde{\widetilde{D}}_1^{\mathrm{T}}(K_1^{\mathrm{T}}P_1 + P_1K_1)\widetilde{\widetilde{D}}_1 + 2\widetilde{\widetilde{D}}_1^{\mathrm{T}}P_1K_1^*\Phi_1^{\mathrm{T}}\Xi_1^*,\end{aligned} \tag{51}$$

Invoking **Lemma 1**, one can obtain

$$2\widetilde{\widetilde{D}}_1^{\mathrm{T}}P_1D_1^* \leq \widetilde{\widetilde{D}}_1^{\mathrm{T}}P_1^2\widetilde{\widetilde{D}}_1 + ||D_1^*||^2, \tag{52}$$

$$\frac{3}{2}e_2^{\mathrm{T}}e_2G_V^{\mathrm{T}}G_V \leq \frac{3}{4}e_2^{\mathrm{T}}A_2e_2||G_V||^4 + \frac{3}{4}, \tag{53}$$

$$2\widetilde{\widetilde{D}}_1^{\mathrm{T}}P_1K_1^*\Phi_1^{\mathrm{T}}\Xi_1^* \leq \vartheta_1^2||\widetilde{\widetilde{D}}_1||^2 + ||\Phi_1||^2, \tag{54}$$

where $||P_1|| \cdot ||K_1^*|| \cdot ||\Xi_1^*|| \leq \vartheta_1$.

Substituting (52)–(54) into (51) yields

$$\begin{aligned}\mathcal{L}W_2 \leq & e_2^{\mathrm{T}}A_2(\Sigma_1/m + G + \Lambda_1^{-1}\omega_1^{\mathrm{T}}\Xi_1 + D_1 - \dot{\delta}_2 + k_{\rho_2}\rho_2 \\ & + \frac{3}{4}e_2||G_V||^4) - \frac{1}{\gamma_1}\mathrm{tr}(\widetilde{\omega}_1^{\mathrm{T}}\dot{\hat{\omega}}_1) + ||D_1^*||^2 + ||\Phi_1||^2 \\ & + \widetilde{\widetilde{D}}_1^{\mathrm{T}}(K_1^{\mathrm{T}}P_1 + P_1K_1 + P_1^2 + \vartheta_1^2I_{3r})\widetilde{\widetilde{D}}_1 + \frac{3}{4},\end{aligned} \tag{55}$$

The adaptive law and actual controller are given as

$$\dot{\hat{\omega}}_1 = \gamma_1\Xi_1e_2^{\mathrm{T}}A_2\Lambda_1^{-1} - \xi_1\hat{\omega}_1, \tag{56}$$

$$\begin{aligned}\Sigma_1 = m(&-h_{21}A_2^{2J-1}e_2 - h_{22}A_2^{2\ell-1}e_2 + \dot{\delta}_2 - k_{\rho_2}\rho_2 - \frac{1}{4}e_2 \\ &-G - \Lambda_1^{-1}\hat{\omega}_1^{\mathrm{T}}\Xi_1 - \hat{D}_1 - \frac{1}{2}A_2e_2 - \frac{3}{4}e_2||G_V||^4),\end{aligned} \tag{57}$$

where $\xi_i > 0, (i = 1, 2)$ are design constants.

Substituting (56) into (55) yields

$$\begin{aligned}\mathcal{L}W_2 \leq & e_2^{\mathrm{T}}A_2(-h_{21}A_2^{2J-1}e_2 - h_{22}A_2^{2\ell-1}e_2 + \dot{\delta}_2 - k_{\rho_2}\rho_2 - \frac{1}{4}e_2 - G - \Lambda_1^{-1}\hat{\omega}_1^{\mathrm{T}}\Xi_1 - \hat{D}_1 \\ & - \frac{1}{2}A_2e_2 - \frac{3}{4}e_2||G_V||^4 + G + \Lambda_1^{-1}\omega_1^{\mathrm{T}}\Xi_1 + D_1 - \dot{\delta}_2 + k_{\rho_2}\rho_2 + \frac{3}{4}e_2||G_V||^4) \\ & - \frac{1}{\gamma_1}\mathrm{tr}(\widetilde{\omega}_1^{\mathrm{T}}(\gamma_1\Xi_1e_2^{\mathrm{T}}A_2\Lambda_1^{-1} - \xi_1\hat{\omega}_1)) + ||D_1^*||^2 + ||\Phi_1||^2 + \widetilde{\widetilde{D}}_1^{\mathrm{T}}(K_1^{\mathrm{T}}P_1 \\ & + P_1K_1 + P_1^2 + \vartheta_1^2I_{3r})\widetilde{\widetilde{D}}_1 + \frac{3}{4} \\ = & -e_2^{\mathrm{T}}h_{21}A_2^{2J-1}e_2 - e_2^{\mathrm{T}}h_{21}A_2^{2\ell-1}e_2 + \frac{\xi_1}{\gamma_1}\mathrm{tr}(\omega_1^{\mathrm{T}}\hat{\omega}_1) + e_2^{\mathrm{T}}A_2\left(A_2e_2 + \widetilde{D}_1 - \frac{1}{4}e_2\right) \\ & + ||D_1^*||^2 + \frac{3}{4} + ||\Phi_1||^2 + \widetilde{\widetilde{D}}_1^{\mathrm{T}}(K_1^{\mathrm{T}}P_1 + P_1K_1 + P_1^2 + \vartheta_1^2I_{3r})\widetilde{\widetilde{D}}_1.\end{aligned} \tag{58}$$

Utilizing **Lemma 1** yields $e_2^{\mathrm{T}} A_2 \widetilde{D}_1 \leq \frac{1}{2} e_2^{\mathrm{T}} A_2^2 e_2 + \frac{1}{2} \widetilde{D}_1^{\mathrm{T}} \widetilde{D}_1$. Then, (58) can be rewritten as

$$\begin{aligned} \mathcal{L}W_2 = & -e_2^{\mathrm{T}} h_{21} A_2^{2j-1} e_2 - e_2^{\mathrm{T}} h_{21} A_2^{2\ell-1} e_2 + e_2^{\mathrm{T}} A_2 \Big(-\frac{1}{2} A_2 \Lambda_2^{-2} e_2 \\ & A_2 e_2 + \widetilde{D}_1 - \frac{1}{4} e_2 \Big) + \frac{\xi_1}{\gamma_1} \mathrm{tr}(\omega_1^{\mathrm{T}} \hat{\omega}_1) + ||D_1^*||^2 + \frac{3}{4} \\ & + ||\Phi_1||^2 + \widetilde{D}_1^{\mathrm{T}} (K_1^{\mathrm{T}} P_1 + P_1 K_1 + P_1^2 + \vartheta_1^2 I_{3r} + G_1) \widetilde{D}_1. \end{aligned} \tag{59}$$

where $G_1 = \mathrm{diag}\{\frac{1}{2} I_3 : 0_3; \cdots, 0_3\} \in \Re^{3r \times 3r}$.

To determine T_{mr}, ϕ_d and θ_d, from $\Sigma_1 = R F_V \in \Re^3 = [\Sigma_{11}, \Sigma_{12}, \Sigma_{13}]^{\mathrm{T}}$, one has:

$$\begin{cases} \theta_d = \arctan[(\Sigma_{11} \cos \psi_d + \Sigma_{12} \sin \psi_d)/\Sigma_{13}] \\ \phi_d = \arctan[\cos \theta_d (\Sigma_{11} \sin \psi_d - \Sigma_{12} \cos \psi_d)/\Sigma_{13}] \\ T_{mr} = -\Sigma_{13}/(\cos \phi_d \cos \theta_d). \end{cases} \tag{60}$$

Step 3: Considering (24) and (25), (30) and (31) obtains

$$de_3 = (He_4 - \dot{\delta}_3 + \alpha_2 + k_{\rho_3} \rho_3) dt. \tag{61}$$

The Lyapunov function is designed as

$$W_3 = \frac{1}{4} (e_3^{\mathrm{T}} e_3)^2. \tag{62}$$

Invoking (71) and (72) produces

$$\mathcal{L}W_3 \leq e_3^{\mathrm{T}} A_3 (He_4 - \dot{\delta}_3 + \alpha_2 + k_{\rho_3} \rho_3), \tag{63}$$

where $A_3 = \mathrm{diag}\{e_{31}; e_{32}; e_{33}\}$.

Invoking **Lemma 1**, one can obtain

$$e_3^{\mathrm{T}} A_3 He_4 \leq \frac{3}{4} e_3^{\mathrm{T}} A_3 H^4 e_3 + \frac{1}{4} e_4^{\mathrm{T}} A_4 e_4, \tag{64}$$

where $A_4 = \mathrm{diag}\{e_{41}; e_{42}; e_{43}\}$.

By employing (73)–(76), one yields

$$\mathcal{L}W_3 \leq e_3^{\mathrm{T}} A_3 (-\dot{\delta}_3 + k_{\rho_3} \rho_3 + \alpha_2 + \frac{3}{4} H^4 e_3) + \frac{1}{4} e_4^{\mathrm{T}} A_4 e_4. \tag{65}$$

Choose the virtual controller as

$$\alpha_2 = -h_{31} A_3^{2j-1} e_3 - h_{32} A_3^{2\ell-1} e_3 + \dot{\delta}_3 - k_{\rho_3} \rho_3 - \frac{3}{4} H^4 e_3. \tag{66}$$

Substituting (80) into (78) yields

$$\begin{aligned} \mathcal{L}W_3 \leq & e_3^{\mathrm{T}} A_3 (-\dot{\delta}_3 + k_{\rho_3} \rho_3 + -h_{31} A_3^{2j-1} e_3 - h_{32} A_3^{2\ell-1} e_3 + \dot{\delta}_3 \\ & - k_{\rho_3} \rho_3 - \frac{3}{4} H^4 e_3 + \frac{3}{4} H^4 e_3) + \frac{1}{4} e_4^{\mathrm{T}} A_4 e_4 \\ = & -e_3^{\mathrm{T}} h_{31} A_3^{2j-1} e_3 - e_3^{\mathrm{T}} h_{32} A_3^{2\ell-1} e_3 + \frac{1}{4} e_4^{\mathrm{T}} A_4 e_4. \end{aligned} \tag{67}$$

Step 4: According to (3), (25) and (31), one can be obtain

$$de_4 = (-F_\mu + \Lambda_2^{-1} \omega_2^{\mathrm{T}} \Xi_2 + J^{-1} \Sigma_2 + D_2 - \dot{\delta}_4 + k_{\rho_4} \rho_4) dt. \tag{68}$$

In order to approximate the external disturbances D_2, the HODO is constructed as

$$\begin{cases} \hat{D}_1 = \eta_{21} + k_{21}X_2, \\ \dot{\eta}_{21} = -k_{21}\Big(-F_\mu + J^{-1}\Sigma_2 + \hat{D}_2 + \Lambda_2^{-1}\omega_2^{\mathrm{T}}\Xi_2\Big) + \dot{\hat{D}}_2, \\ \dot{\hat{D}}_2 = \eta_{22} + k_{22}X_2, \\ \dot{\eta}_{22} = -k_{22}\Big(-F_\mu + J^{-1}\Sigma_2 + \hat{D}_2 + \Lambda_2^{-1}\omega_2^{\mathrm{T}}\Xi_2\Big) + \ddot{\hat{D}}_2, \\ \cdots \\ \hat{D}_2^{(r-1)} = \eta_{2r} + k_{2r}X_2, \\ \dot{\eta}_{2r} = -k_{2r}\Big(-F_\mu + J^{-1}\Sigma_2 + \hat{D}_2 + \Lambda_2^{-1}\omega_2^{\mathrm{T}}\Xi_2\Big), \end{cases} \tag{69}$$

where $\hat{D}_2 \in \Re^3, \dot{\hat{D}}_2 \in \Re^3, \ldots, \hat{D}_2^{(r-1)} \in \Re^3$ are the estimates of $D_2, \dot{D}_2, \ldots, D_2^{(r-1)}$. $\eta_{2r} \in \Re^3$ are auxiliary variables, $k_{2r} \in \Re^{3\times 3} \succ 0$ are design matrices and $\dot{X}_2 = -F_\mu + J^{-1}\Sigma_2 + \Lambda_2^{-1}\omega_2^{\mathrm{T}}\Xi_2 + D_2$.

Defining $\widetilde{\bar{D}}_2 = [\widetilde{D}_2^{\mathrm{T}}, \dot{\widetilde{D}}_2^{\mathrm{T}}, \ldots, (\widetilde{D}_2^{r-1})^{\mathrm{T}}]^{\mathrm{T}}$ with $\widetilde{D}_2^s = D_2^s - \hat{D}_2^s, (s = 1, 2, \cdots, r-1)$, then one can obtain

$$\dot{\widetilde{\bar{D}}}_2 = K_2\widetilde{\bar{D}}_2 + D_2^* + K_2^*\Phi_2^{\mathrm{T}}\Xi_2^*, \tag{70}$$

where $K_2^* = \mathrm{diag}\{k_{21}; k_{22}; \cdots, k_{2r}\}$,

$$D_2^* = \begin{bmatrix} 0 \\ 0 \\ \vdots \\ D_2^r \end{bmatrix}, \qquad K_2 = \begin{bmatrix} k_{21} & I_3 & \cdots & 0 & 0 \\ k_{22} & 0_3 & I_3 & \cdots & 0_3 \\ \vdots & \vdots & \vdots & \cdots & \vdots \\ k_{2r} & 0_3 & 0_3 & \cdots & 0 \end{bmatrix},$$

and K_2 is a Hurwitz matrix. Thus, there are positive definite matrices $P_2 = P_2^{\mathrm{T}} \in \Re^{3r\times 3r}$, and one can obtain

$$K_2^{\mathrm{T}}P_2 + P_2K_2 = -Q_2, \tag{71}$$

where $Q_2 = Q_2^{\mathrm{T}} \in \Re^{3r\times 3r}$ is a positive definite matrix.

The Lyapunov function is constructed as

$$W_4 = \frac{1}{4}(e_4^{\mathrm{T}}e_4)^2 + \widetilde{\bar{D}}_2^{\mathrm{T}}P_2\widetilde{\bar{D}}_2 + \frac{1}{2\gamma_2}\mathrm{tr}(\widetilde{\omega}_2\widetilde{\omega}_2). \tag{72}$$

Taking the derivative of W_4 yields

$$\begin{aligned} \mathcal{L}W_4 \leq & e_4^{\mathrm{T}}A_4(-F_\mu + \Lambda_2^{-1}\omega_2^{\mathrm{T}}\Xi_2 + D_2 - \dot{\delta}_4 + k_{\rho_4}\rho_4) \\ & + \frac{3}{2}e_2^{\mathrm{T}}e_2G_\mu^{\mathrm{T}}G_\mu - \frac{1}{\gamma_2}\mathrm{tr}(\widetilde{\omega}_2^{\mathrm{T}}\dot{\hat{\omega}}_2) + 2\widetilde{\bar{D}}_2^{\mathrm{T}}P_2D_2^* \\ & + \widetilde{\bar{D}}_2^{\mathrm{T}}(K_2^{\mathrm{T}}P_2 + P_2K_2)\widetilde{\bar{D}}_2 + 2\widetilde{\bar{D}}_2^{\mathrm{T}}P_2K_2^*\Phi_2^{\mathrm{T}}\Xi_2^*, \end{aligned} \tag{73}$$

Employing **Lemma 1**, one can obtain

$$2\widetilde{\widetilde{D}}_2^{\mathrm{T}} P_2 D_2^* \le \widetilde{\widetilde{D}}_2^{\mathrm{T}} P_2^2 \widetilde{\widetilde{D}}_2 + ||D_2^*||^2, \tag{74}$$

$$\frac{3}{2} e_4^{\mathrm{T}} e_4 G_\mu^{\mathrm{T}} G_\mu \le \frac{3}{4} e_4^{\mathrm{T}} A_4 e_4 ||G_\mu||^4 + \frac{3}{4}, \tag{75}$$

$$2\widetilde{\widetilde{D}}_2^{\mathrm{T}} P_2 K_2^* \Phi_2^{\mathrm{T}} \Xi_2^* \le \vartheta_2^2 ||\widetilde{\widetilde{D}}_2||^2 + ||\Phi_2||^2, \tag{76}$$

where $||P_2|| \cdot ||K_2^*|| \cdot ||\Xi_2^*|| \le \vartheta_2$.

Then, (73) can be rewritten as

$$\begin{aligned} \mathcal{L}W_4 \le & e_4^{\mathrm{T}} A_4 \Big(-F_\mu + J^{-1}\Sigma_2 + \Lambda_2^{-1}\omega_2^{\mathrm{T}}\Xi_2 + D_2 - \dot{\delta}_4 + k_{\rho_4}\rho_4 \\ & + \frac{3}{4} e_4 ||G_\mu||^4 \Big) - \frac{1}{\gamma_2}\mathrm{tr}(\widetilde{\omega}_2^{\mathrm{T}}\dot{\hat{\omega}}_2) + ||D_2^*||^2 + ||\widetilde{\Phi}_2||^2 \\ & + \widetilde{\widetilde{D}}_2^{\mathrm{T}}(K_2^{\mathrm{T}} P_2 + P_2 K_2 + P_2^2 + \vartheta_2^2 I_{3r})\widetilde{\widetilde{D}}_2 + \frac{3}{4}, \end{aligned} \tag{77}$$

Select the adaptive law and actual controller as

$$\dot{\hat{\omega}}_2 = \gamma_2 \Xi_2 e_4^{\mathrm{T}} A_4 \Lambda_2^{-1} - \xi_2 \hat{\omega}_2, \tag{78}$$

$$\begin{aligned} \Sigma_2 = J^{-1}\Big(& -h_{41} A_4^{2J-1} e_4 - h_{42} A_4^{2\ell-1} e_4 + \dot{\delta}_4 - k_{\rho_4}\rho_4 + F_\mu \\ & - \frac{1}{4} e_4 - \Lambda_2^{-1}\hat{\omega}_2^{\mathrm{T}}\Xi_2 - \hat{D}_2 - \frac{1}{2} A_4 e_4 - \frac{3}{4} e_4 ||G_\mu||^4 \Big). \end{aligned} \tag{79}$$

Substituting (78) and (79) into (77) yields

$$\begin{aligned} \mathcal{L}W_4 \le & e_4^{\mathrm{T}} A_4 (-F_\mu - h_{41} A_4^{2J-1} e_4 - h_{42} A_4^{2\ell-1} e_4 + \dot{\delta}_4 - k_{\rho_4}\rho_4 + F_\mu \\ & - \frac{1}{4} e_4 - \Lambda_2^{-1}\hat{\omega}_2^{\mathrm{T}}\Xi_2 - \hat{D}_2 - \frac{1}{2} A_4 e_4 - \frac{3}{4} e_4 ||G_\mu||^4 + \Lambda_2^{-1}\omega_2^{\mathrm{T}}\Xi_2 \\ & + D_2 - \dot{\delta}_4 + k_{\rho_4}\rho_4 + \frac{3}{4} e_4 ||G_\mu||^4) - \frac{1}{\gamma_2}\mathrm{tr}(\widetilde{\omega}_2^{\mathrm{T}}(\gamma_2 \Xi_2 e_4^{\mathrm{T}} A_4 \Lambda_2^{-1} - \xi_2 \hat{\omega}_2)) \\ & + ||D_2^*||^2 + ||\widetilde{\Phi}_2||^2 + \widetilde{\widetilde{D}}_2^{\mathrm{T}}(K_2^{\mathrm{T}} P_2 + P_2 K_2 + P_2^2 + \vartheta_2^2 I_{3r})\widetilde{\widetilde{D}}_2 + \frac{3}{4} \\ = & - e_2^{\mathrm{T}} h_{41} A_4^{2J-1} e_4 - e_4^{\mathrm{T}} h_{41} A_4^{2\ell-1} e_4 + \frac{\xi_2}{\gamma_2}\mathrm{tr}(\omega_2^{\mathrm{T}}\hat{\omega}_2) + e_4^{\mathrm{T}} A_4 \Big(A_4 e_4 + \widetilde{D}_2 - \frac{1}{4} e_4 \Big) \\ & + ||D_2^*||^2 + \frac{3}{4} + ||\Phi_2||^2 + \widetilde{\widetilde{D}}_2^{\mathrm{T}}(K_2^{\mathrm{T}} P_2 + P_2 K_2 + P_2^2 + \vartheta_2^2 I_{3r})\widetilde{\widetilde{D}}_2. \end{aligned} \tag{80}$$

Utilizing **Lemma 1** yields $e_4^{\mathrm{T}} A_4 \widetilde{D}_2 \le \frac{1}{2} e_4^{\mathrm{T}} A_4^2 e_4 + \frac{1}{2}\widetilde{D}_2^{\mathrm{T}}\widetilde{D}_2$. Then, (80) can be rewritten as

$$\begin{aligned} \mathcal{L}W_4 = & - e_4^{\mathrm{T}} h_{41} A_4^{2J-1} e_4 - e_4^{\mathrm{T}} h_{41} A_4^{2\ell-1} e_4 + e_4^{\mathrm{T}} A_4 \Big(-\frac{1}{2} A_4 \Lambda_2^{-2} e_4 \\ & A_4 e_4 + \widetilde{D}_2 - \frac{1}{4} e_4 \Big) + \frac{\xi_2}{\gamma_2}\mathrm{tr}(\omega_2^{\mathrm{T}}\hat{\omega}_2) + ||D_2^*||^2 + \frac{3}{4} \\ & + ||\Phi_2||^2 + \widetilde{\widetilde{D}}_2^{\mathrm{T}}(K_2^{\mathrm{T}} P_2 + P_2 K_2 + P_2^2 + \vartheta_2^2 I_{3r} + G_2)\widetilde{\widetilde{D}}_2. \end{aligned} \tag{81}$$

where $G_2 = \mathrm{diag}\{\frac{1}{2} I_3 : 0_3; \cdots, 0_3\} \in \Re^{3r \times 3r}$.

4. Stability Analysis

This section provides the following theorem to perform the effectiveness of the controller.

Theorem 2. *For the uncertain UAH system with random disturbances and external disturbances. If the second-order DSC is selected as (14), the virtual controller and actual controller are selected as (44), (57), (66) and (79), the adaptive laws are constructed as (56) and (78), the command filters are provided as (14), (26)–(29) and the HODOs are designed as (47) and (69), then based on the SPA, the proposed control scheme ensures that all states of the unmanned helicopter are semi-globally fixed-time stable in probability. In addition, the convergence time only depends on the designed parameters.*

Proof. Defining $W = \sum_{j=1}^{4} W_i$, one has

$$\begin{aligned}\mathcal{L}W \leq & -a_1 \sum_{j=1}^{4} e_j^{\mathrm{T}} A_j^{2J-1} e_j - a_1 \sum_{j=1}^{4} e_j^{\mathrm{T}} A_j^{2\ell-1} e_j + a_1 \sum_{j=1}^{2} \frac{1}{\gamma_j} \mathrm{tr}(\varpi_j^{\mathrm{T}} \hat{\varpi}_j) \\ & - a_1 \sum_{j=1}^{2} (\widetilde{\bar{D}}_j^{\mathrm{T}} P_j \widetilde{\bar{D}}_j)^2 + M_1, \end{aligned} \tag{82}$$

where $a_1 = \min\{\lambda_{\min}(h_{j1}), \lambda_{\min}(h_{j2}), (j = 1,2,3,4).\ \xi_j, \lambda_{\min}(K_j^{\mathrm{T}} P_j + P_j K_j + P_j^2 + \vartheta_j^2 I_{3r} + G_j)/(\lambda_{\max}(P_j))^2, (j = 1,2)\}$ $M_1 = \sum_{j=1}^{2}(||D_j^*||^2 + ||\Phi_2||^2) + 3/2$.

Employing **Lemma 1**, one can obtain

$$\mathrm{tr}(\varpi_j^{\mathrm{T}} \hat{\varpi}_j) \leq \frac{1}{2}\mathrm{tr}(\varpi_j^{\mathrm{T}} \varpi_j) - \frac{1}{2}\mathrm{tr}(\widetilde{\varpi}_j^{\mathrm{T}} \widetilde{\varpi}_j). \tag{83}$$

Then, (82) can be rewritten as

$$\begin{aligned}\mathcal{L}W \leq & -a_2 \sum_{j=1}^{4} e_j^{\mathrm{T}} A_j^{2J-1} e_j - a_2 \sum_{j=1}^{4} e_j^{\mathrm{T}} A_j^{2\ell-1} e_j - a_2 \sum_{j=1}^{2} \frac{1}{\gamma_j} \mathrm{tr}(\widetilde{\varpi}_j^{\mathrm{T}} \widetilde{\varpi}_j) \\ & - a_2 \sum_{j=1}^{2} (\widetilde{\bar{D}}_j^{\mathrm{T}} P_j \widetilde{\bar{D}}_j)^2 + M_2, \end{aligned} \tag{84}$$

where $a_2 = \min\{a_1, \frac{1}{2}a_1\}$, $M_2 = M_1 + \sum_{j=1}^{2} \frac{1}{2}\mathrm{tr}(\varpi_j^{\mathrm{T}} \varpi_j)$.

Employing **Lemma 4** yields

$$-a_2 \sum_{j=1}^{4} e_j^{\mathrm{T}} A_j^{2J-1} e_j \leq -4^J a_2 \left(\frac{1}{4}(e_j^{\mathrm{T}} e_j)^2\right)^J, \tag{85}$$

$$-a_2 \sum_{j=1}^{4} e_j^{\mathrm{T}} B_j^{\ell} A_j^{2\ell-1} e_j \leq -4^{\ell} 12^{1-\ell} a_2 \left(\frac{1}{4}(e_j^{\mathrm{T}} e_j)^2\right)^{\ell}. \tag{86}$$

Invoking (84)–(86) yields

$$\begin{aligned}\mathcal{L}W \leq & -a_3 \sum_{j=1}^{4} \left(\frac{1}{4}(e_j^{\mathrm{T}} e_j)^2\right)^J - a_3 \sum_{j=1}^{4} \left(\frac{1}{4}(e_j^{\mathrm{T}} e_j)^2\right)^{\ell} \\ & - a_3 \sum_{j=1}^{2} \frac{1}{\gamma_j} \mathrm{tr}(\widetilde{\varpi}_j^{\mathrm{T}} \widetilde{\varpi}_j) - 2a_3 \sum_{j=1}^{2} (\widetilde{\bar{D}}_j^{\mathrm{T}} P_j \widetilde{\bar{D}}_j)^2 + M_2 \\ & - a_3 \left(\sum_{j=1}^{2} \frac{1}{2\gamma_j} \mathrm{tr}(\widetilde{\varpi}_j^{\mathrm{T}} \widetilde{\varpi}_j)\right)^J - a_3 \left(\sum_{j=1}^{2} \widetilde{\bar{D}}_j^{\mathrm{T}} P_j \widetilde{\bar{D}}_j^2\right)^J \\ & + a_3 \left(\sum_{j=1}^{2} \frac{1}{2\gamma_j} \mathrm{tr}(\widetilde{\varpi}_j^{\mathrm{T}} \widetilde{\varpi}_j)\right)^J + a_3 \left(\sum_{j=1}^{2} \widetilde{\bar{D}}_j^{\mathrm{T}} P_j \widetilde{\bar{D}}_j^2\right)^J. \end{aligned} \tag{87}$$

where $a_3 = \min\{a_2/2, 4^{\jmath}a_2, 4^{\ell}12^{(1-\ell)}a_2\}$.

Employing **Lemma 1**, one can obtain

$$a_3\left(\widetilde{\widetilde{D}}_j^{\mathrm{T}} P_j \widetilde{\widetilde{D}}_j\right)^{\jmath} \leq a_3(1-\jmath)\jmath^{\frac{\jmath}{1-\jmath}} + \sum_{j=1}^{2}(\widetilde{\widetilde{D}}_j^{\mathrm{T}} P_j \widetilde{\widetilde{D}}_j)^2, \tag{88}$$

$$a_3\left(\sum_{j=1}^{2}\frac{1}{2\gamma_j}\mathrm{tr}(\widetilde{\omega}_j^{\mathrm{T}}\widetilde{\omega}_j)\right)^{\jmath} \leq a_3(1-\jmath)\jmath^{\frac{\jmath}{1-\jmath}} + \sum_{j=1}^{2}\frac{1}{2\gamma_j}\mathrm{tr}(\widetilde{\omega}_j^{\mathrm{T}}\widetilde{\omega}_j). \tag{89}$$

Invoking (88) and (89), (87) can be rewritten as

$$\begin{aligned}\mathcal{L}W \leq & -a_3\left(\frac{1}{4}(e_j^{\mathrm{T}}e_j)^2\right)^{\jmath} - a_3\left(\frac{1}{4}(e_j^{\mathrm{T}}e_j)^2\right)^{\ell} \\ & - a_3\sum_{j=1}^{2}\frac{1}{2\gamma_j}\mathrm{tr}(\widetilde{\omega}_j^{\mathrm{T}}\widetilde{\omega}_j) - a_3\sum_{j=1}^{2}(\widetilde{\widetilde{D}}_j^{\mathrm{T}} P_j \widetilde{\widetilde{D}}_j)^2 + M_3 \\ & - a_3\left(\sum_{j=1}^{2}\frac{1}{2\gamma_j}\mathrm{tr}(\widetilde{\omega}_j^{\mathrm{T}}\widetilde{\omega}_j)\right)^{\jmath} - a_3\left(\sum_{j=1}^{2}\widetilde{\widetilde{D}}_j^{\mathrm{T}} P_j \widetilde{\widetilde{D}}_j\right)^{\jmath}.\end{aligned} \tag{90}$$

where $M_3 = M_2 + 2a_3(1-\iota)\iota^{\frac{\iota}{1-\iota}}$.

Assuming $(\widetilde{\widetilde{D}}_j^{\mathrm{T}} P_j \widetilde{\widetilde{D}}_j)^2 \leq 1$ and $\mathrm{tr}(\omega_j^{\mathrm{T}}\omega_j) \leq 2\gamma_j$, then one can obtain

$$-\sum_{j=1}^{2}(\widetilde{\widetilde{D}}_j^{\mathrm{T}} P_j \widetilde{\widetilde{D}}_j)^2 \leq \left(\sum_{j=1}^{2}(\widetilde{\widetilde{D}}_j^{\mathrm{T}} P_j \widetilde{\widetilde{D}}_j)^2\right)^{\ell}, \tag{91}$$

$$-\sum_{j=1}^{2}\frac{1}{2\gamma_j}\mathrm{tr}(\widetilde{\omega}_j^{\mathrm{T}}\widetilde{\omega}_j) \leq \left(\sum_{j=1}^{2}\frac{1}{2\gamma_j}\mathrm{tr}(\widetilde{\omega}_j^{\mathrm{T}}\widetilde{\omega}_j)\right)^{\ell}. \tag{92}$$

Employing (91) and (92), (90) can be rewritten as

$$\begin{aligned}\mathcal{L}W \leq & -a_3\left(\frac{1}{4}(e_j^{\mathrm{T}}e_j)^2\right)^{\jmath} - a_3\left(\frac{1}{4}(e_j^{\mathrm{T}}e_j)^2\right)^{\ell} \\ & - a_3\left(\sum_{j=1}^{2}\widetilde{\widetilde{D}}_j^{\mathrm{T}} P_j \widetilde{\widetilde{D}}_j\right)^{\ell} - a_3\left(\sum_{j=1}^{4}\frac{1}{2\gamma_j}\mathrm{tr}(\widetilde{\omega}_j^{\mathrm{T}}\widetilde{\omega}_j)\right)^{\ell} \\ & - a_3\left(\sum_{j=1}^{4}\frac{1}{2\gamma_j}\mathrm{tr}(\widetilde{\omega}_j^{\mathrm{T}}\widetilde{\omega}_j)\right)^{\jmath} - a_3\left(\sum_{j=1}^{2}\widetilde{\widetilde{D}}_j^{\mathrm{T}} P_j \widetilde{\widetilde{D}}_j\right)^{\jmath} + M_3 \\ = & -KV^{\jmath} - LV^{\ell} + M.\end{aligned} \tag{93}$$

where $K = a_3$, $L = 3^{1-\ell}a_3$, $M = M_3$.

The proof is concluded. □

5. Simulation

Some necessary parameters are provided, including the following: assume that the unmanned helicopter has 10% uncertainties. The random disturbance coefficient matrices and external disturbance are provided as follows:

$$G_V = \begin{bmatrix} 0.03Y\psi \\ 0.1cos(0.3\psi) \\ 0.006sin(0.6Z) \end{bmatrix}, \quad G_\mu = \begin{bmatrix} 0.01uw \\ 0 \\ 0.02sin(0.1w) \end{bmatrix},$$
$$d_1 = \begin{bmatrix} 1.6cos(0.1t-2) \\ 0.5sin(0.1t+0.3) \\ 0.4cos(0.3t)+0.1cos(0.1t) \end{bmatrix}, \quad d_2 = \begin{bmatrix} 10sin(0.1t) \\ 5sin(0.1t+0.3) \\ 4cos(0.3t)+1cos(0.1t) \end{bmatrix}.$$

Table 1 provides the necessary parameters.

Table 1. Fuselage parameters.

Symbol	Value	Unit
g	9.8	m/s^2
m	800.0	kg
(J_X, J_Y, J_Z)	$(358.4, 777.9, 601.4)$	$kg \cdot m^2$

The desired parameters are provided as $\jmath = 0.8, \ell = 1.1, h_{11} = 0.1\text{diag}\{1;1;1\}$, $h_{12} = 4\text{diag}\{1;1;1\}, h_{21} = 0.01\text{diag}\{1;1;1\}, h_{22} = 1\text{diag}\{1;1;1\}, h_{31} = 0.1\text{diag}\{1;1;1\}$, $h_{32} = 16\text{diag}\{1;1;1\}, h_{41} = 0.01\text{diag}\{1;1;1\}, h_{42} = 6\text{diag}\{1;1;1\}, \sigma_1 = 1\text{diag}\{1;1;1\}$, $\sigma_2 = 0.1\text{diag}\{1;1;1\}, \Gamma_1 = 5\text{diag}\{1;1;1\}, \Gamma_2 = 0.3\text{diag}\{1;1;1\}, \Gamma_3 = 1\text{diag}\{1;1;1\}$, $\Gamma_4 = 0.1\text{diag}\{1;1;1\}, k_{\rho_1} = k_{\rho_2} = k_{\rho_3} = k_{\rho_4} = 2\text{diag}\{1;1;1\}, \Lambda_1 = \Lambda_2 = 3\text{diag}\{1;1;1\}$, $k_{11} = k_{12} = 2\text{diag}\{1;1;1\}, k_{21} = 1.5\text{diag}\{1;1;1\}, k_{22} = 4\text{diag}\{1;1;1\}, \gamma_1 = 1, \gamma_2 = 6$, $\xi_1 = \xi_2 = 1, \nu_1 = 0.5, \nu_2 = \nu_3 = 1$ and $\nu_4 = 0.2$.

For FLS used in this paper, choose the number of rules $k = 11$, and the fuzzy member functions are chosen as

$$\Pi = exp\left(\frac{-(\hbar_i - 12 + 2i)}{10^2}\right), j = 1, 2, , \ldots, 6 \tag{94}$$

$$\Pi = exp\left(\frac{-(\hbar_i - 36 + 2i)}{40^2}\right), j = 7, 8, , \ldots, 12 \tag{95}$$

where $i = 1, 2, \ldots, 11.[\hbar_1, \hbar_2, \hbar_3, \hbar_4, \hbar_5, \hbar_6, \hbar_7, \hbar_8, \hbar_9, \hbar_{10}, \hbar_1 1,\ \hbar_1 2,]^{\mathrm{T}} = [X, Y, Z, u, v, w, \phi, \theta, \psi, p, q, r]^{\mathrm{T}}$.

The initial conditions, desired signals and state constraints are provided in Table 2.

According to the information above, the following figures illustrate the performance of the control scheme.

Figures 3–10 are the state tracking responses of the UAH under the system uncertainties and multisource disturbances, Figures 3–10 correspond to the position, velocity, angle and angular velocity tracking curves of the UAH, respectively. It can be observed from Figures 3 and 7–9 that the position P and attitude Ω of the UAH system are restricted within the time-varying security boundaries, and because of the time-varying margins, P and Ω always maintain a certain range with the security boundaries, which further improves the security of UAH. In addition, the velocity and angular velocity of the UAH system can track the desired signals accurately and quickly, which also meets the requirements of the actual system for fast, accurate and stable.

Table 2. Parameters of simulation.

Symbol	Value	Unit
X_d	$8+3cos(0.1t+0.1)+4sin(0.2t+0.8)$	m
Y_d	$4cos(0.01t+1)+8sin(0.06t)$	m
Z_d	$-12-10cos(0.1t+2)-2sin(0.05t)$	m
ψ_d	0	deg
X_{up}	$14+1sin(0.1t)$	m
X_{low}	$3+0.6cos(0.02t)-1sin(0.2t)$	m
Y_{up}	$9-1.2cos(0.1t)$	m
Y_{low}	$-7+1sin(0.06t)$	m
Z_{up}	-2	m
Z_{low}	$-22+1cos(0.7t)$	m
ϕ_{up}	$11.5+1.15sin(0.1t)$	deg
ϕ_{low}	$-11.5-5.7cos(0.06t)$	deg
θ_{up}	$114.6-11.5cos(0.08t+0.2)$	deg
θ_{low}	45.8	deg
ψ_{up}	17.2	deg
ψ_{low}	-17.2	deg

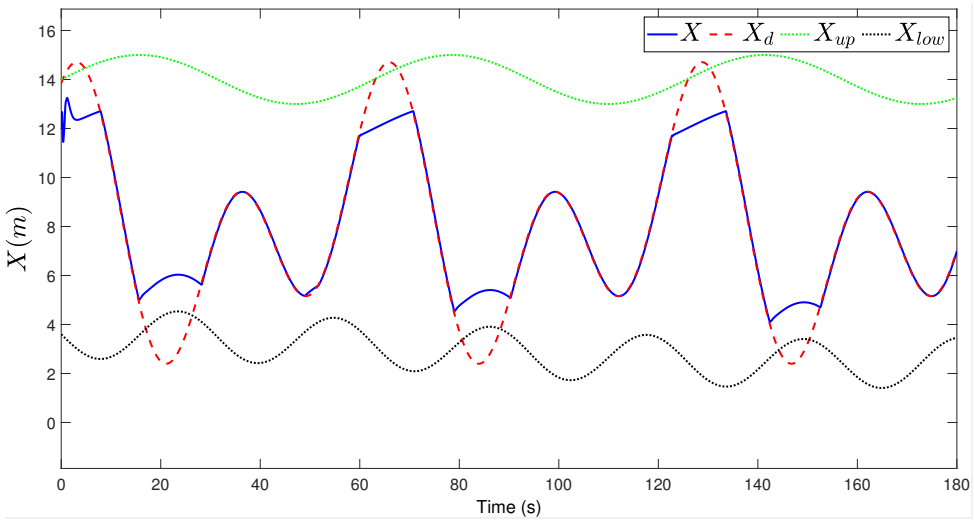

Figure 3. Tracking performance of X-axis.

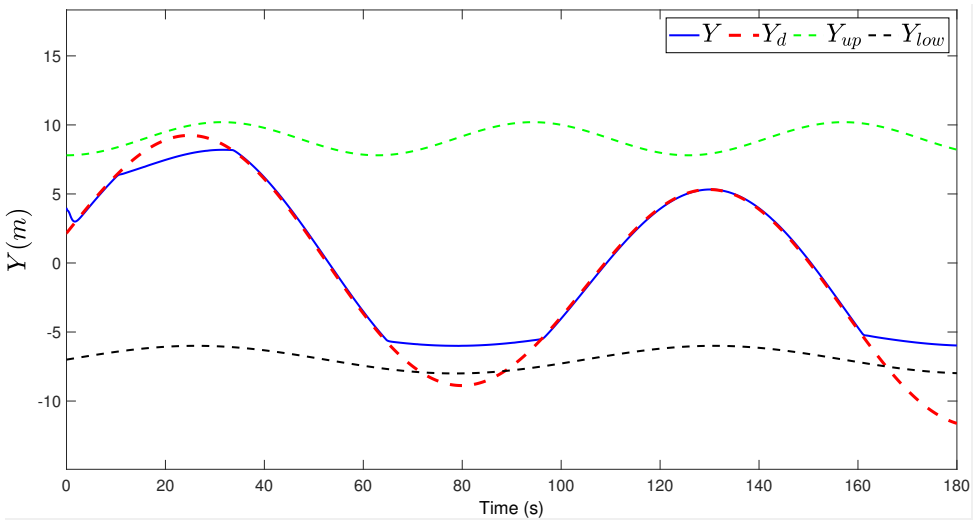

Figure 4. Tracking performance of Y-axis.

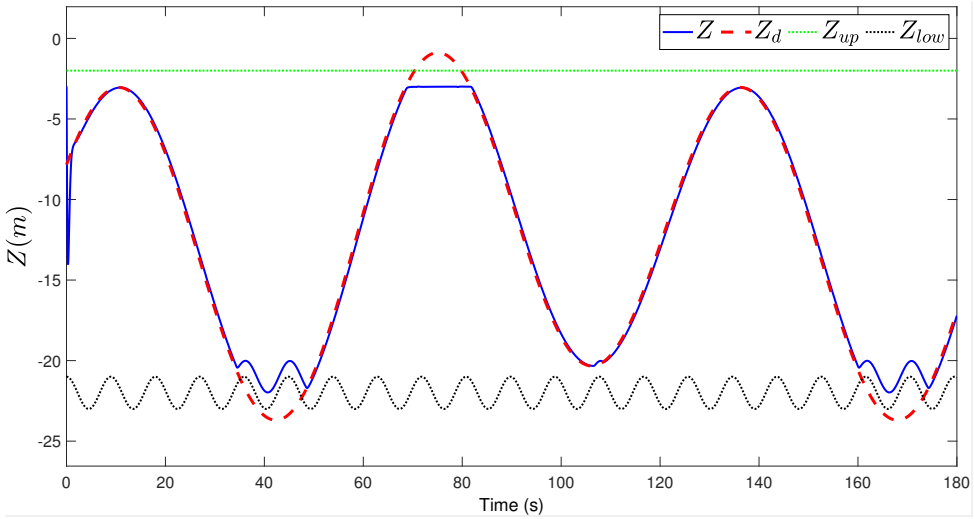

Figure 5. Tracking performance of Z-axis.

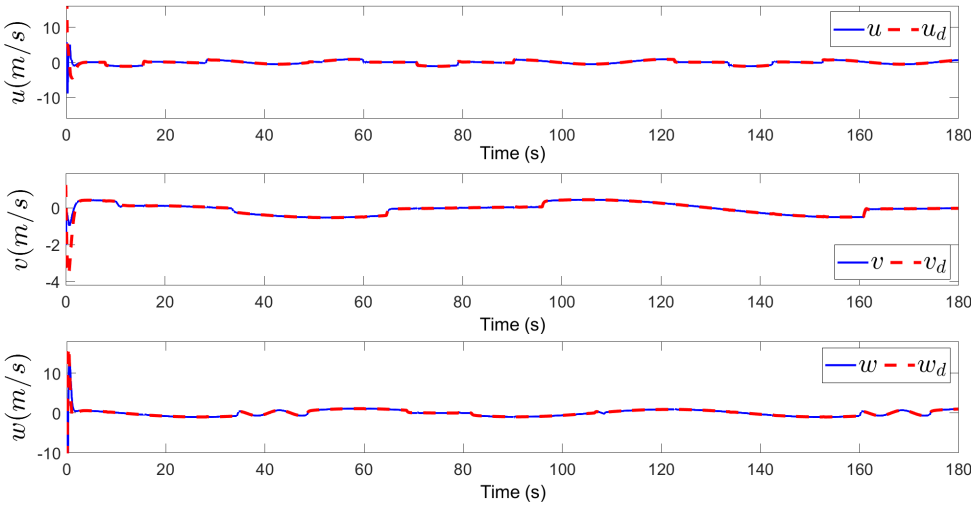

Figure 6. Tracking performance of velocity.

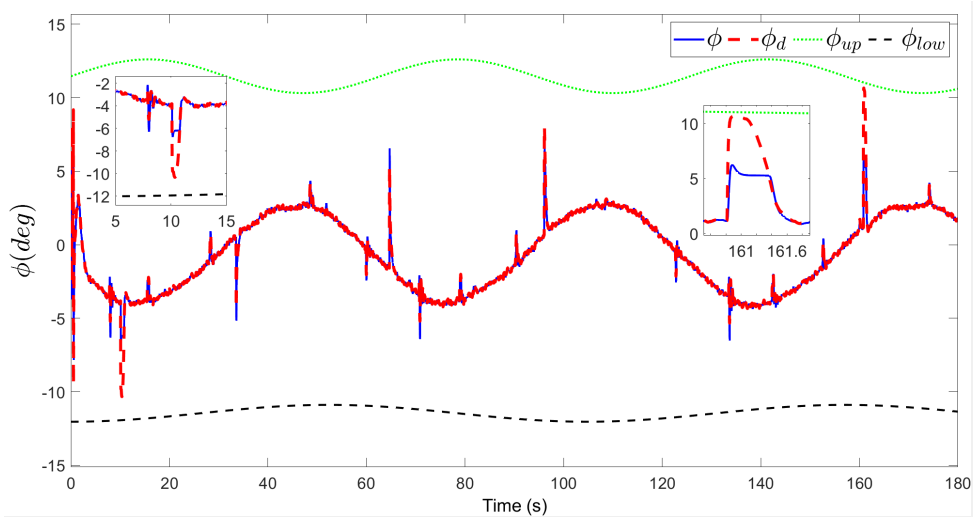

Figure 7. Tracking performance of ϕ.

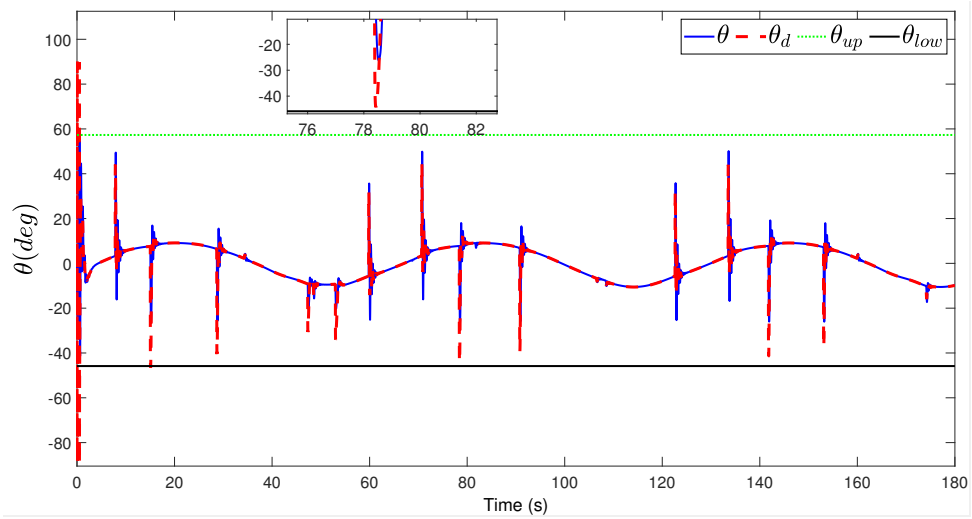

Figure 8. Tracking performance of θ.

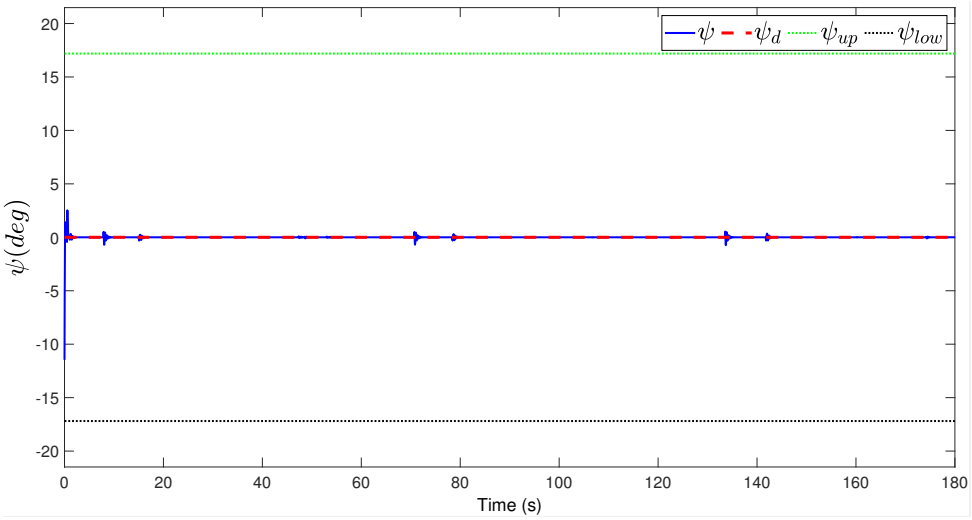

Figure 9. Tracking performance of ψ.

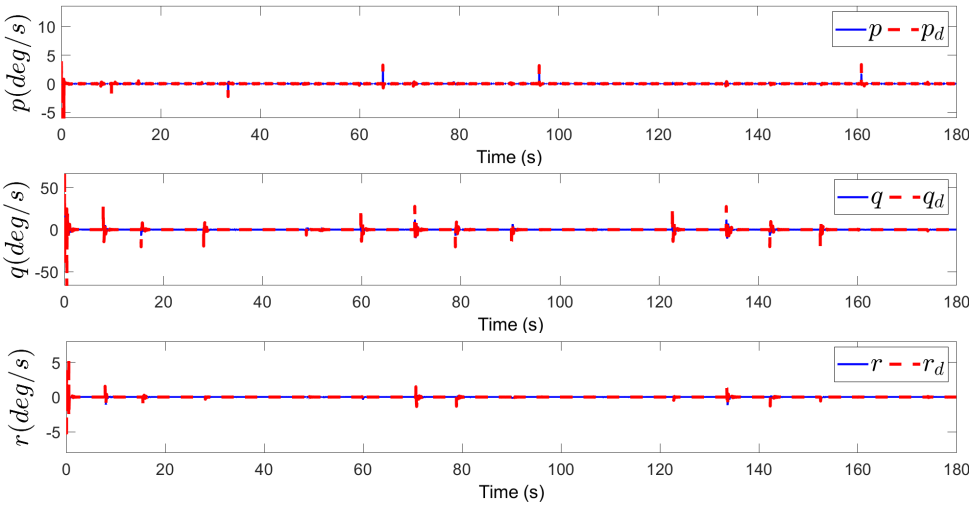

Figure 10. Tracking performance of angular velocity.

Figure 11 stands for the inputs of the system, where, T_{mr}, Σ_X, Σ_X and Σ_Z represent the main rotor pull, yaw moment, pitching moment and rolling moment of UAH, respectively. They work together to realize various maneuvers of the UAH in three-dimensional space. In addition, it can be observed that although there are large vibrations in the $T = 0$ s, they can quickly reach stability, and meet the output range of the actual system.

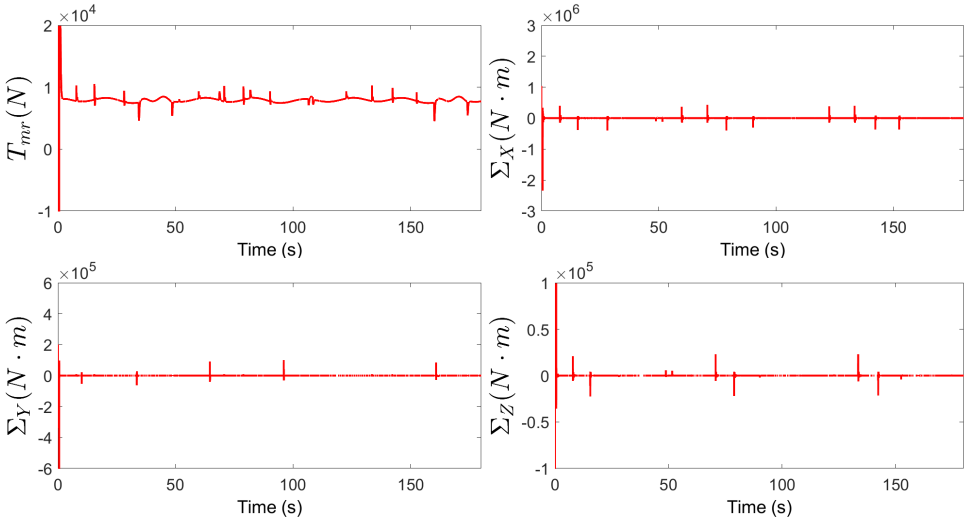

Figure 11. Control inputs of the designed scheme.

Figures 12 and 13 show the tracking errors of position, velocity, angle and angular velocity, respectively. It can be observed that all states of the closed-loop system converge the desired region in fixed-time even through suffering the time-varying safety boundary constraints, stochastic disturbances and external disturbances.

Figures 14 and 15 are the tracking responses of the d_1, d_2 and $\hat{d}_1, \hat{d}_2$. Due to the influence of random disturbance, although there are pulses in the observation process of HODO, the designed observer can still observe the external disturbances quickly and accurately. In addition, compared with the traditional NDO, the HODO obtains the unbiased estimate of the time derivatives of external disturbances, which further improves the observation accuracy of the observer. In order to show the change in the flight trajectory of the unmanned helicopter more clearly, Figure 16 provides a three-dimensional diagram.

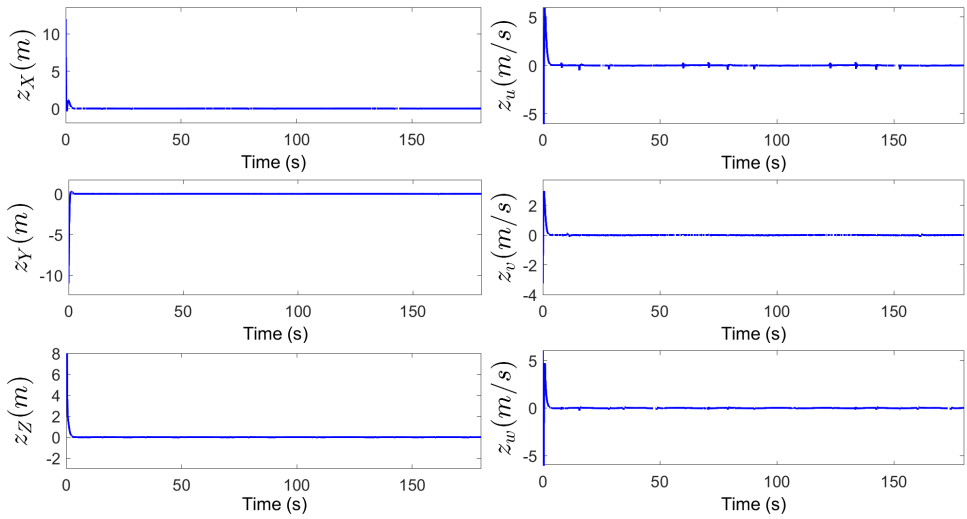

Figure 12. Tracking performance of position subsystem.

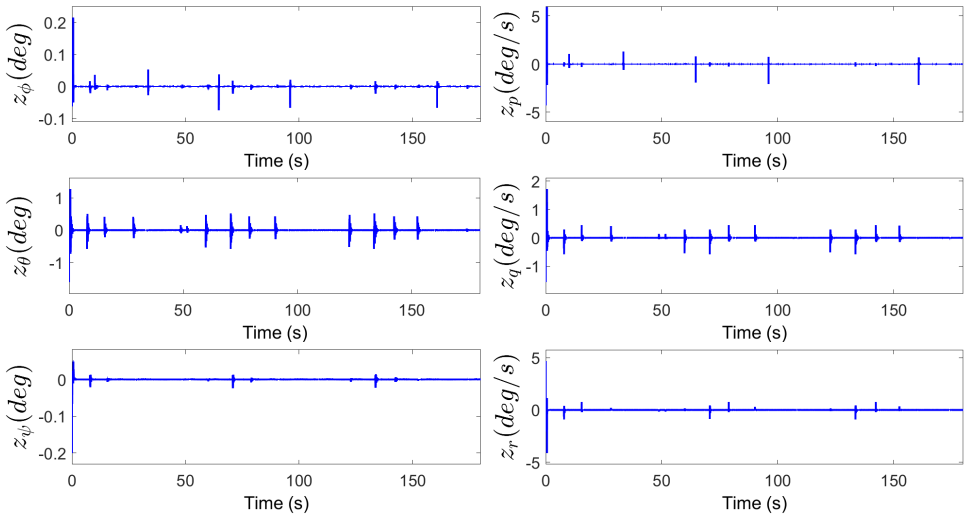

Figure 13. Tracking performance of attitude subsystem.

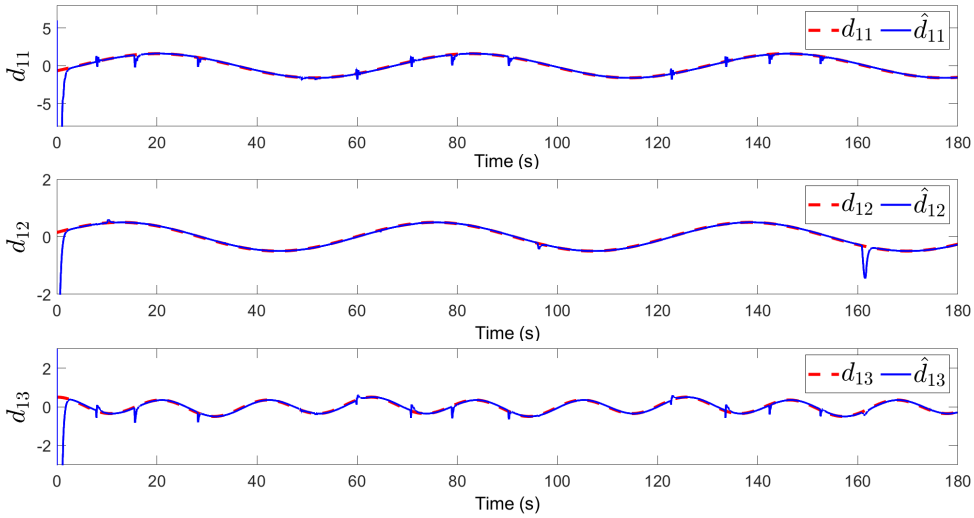

Figure 14. Tracking performance of d_1.

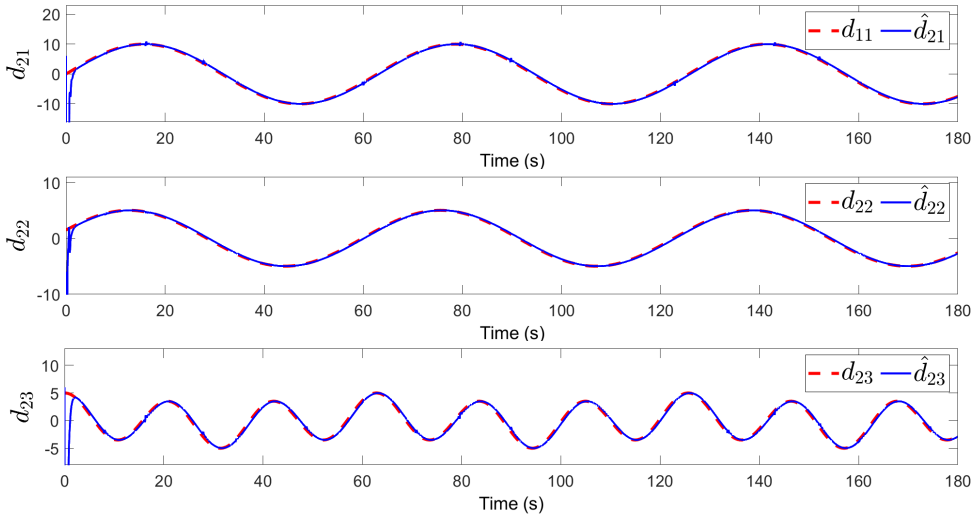

Figure 15. Tracking performance of d_2.

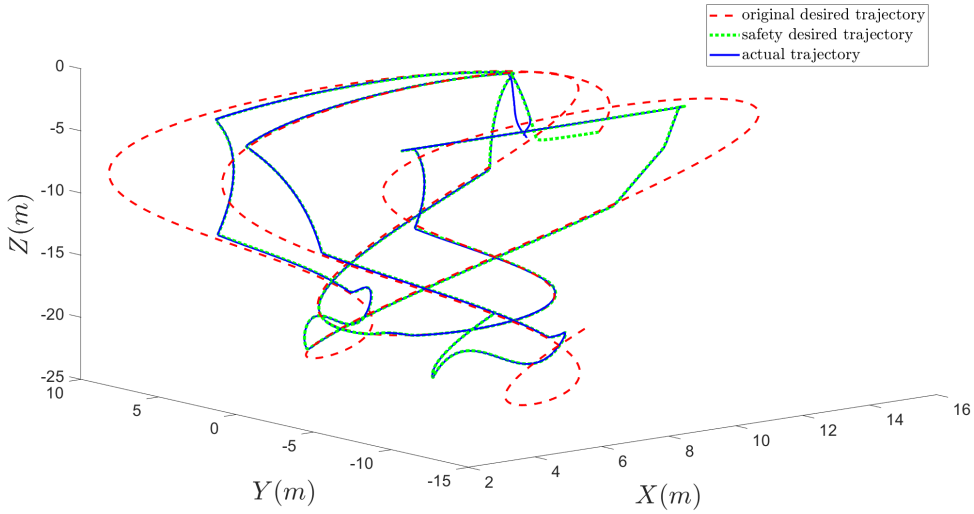

Figure 16. Three-dimensional trajectory diagram.

In addition, in order to show the performance and effect of the designed controller, we provide a comparative experiment, as shown in Figure 17, taking X as an example, which contains the tracking curve obtained by different control methods. It can be observed that although X of the proposed control scheme without FLS can track the desired signal, the oscillation is more severe. X of the control scheme without SPA will cause the UAH system to cross the safety boundaries, which may cause the UAH to collide with the obstacle boundaries during operation or coincide with the airframe crash. Though X of the proposed method in [25] can make the output tracking the desired signal, there is slightly larger error. Although the method proposed by [43] can quickly track the desired signal, FTDO has no way to determine an unbiased estimate of the disturbance, resulting in a slightly larger error. The X of the control scheme without HODO can hardly accurately track the time-varying safety expectation signal. In order to make the comparison more clear, we provide Table 3, including the maximum X-axis error and convergence time information under different methods, which clearly shows the superiority of the control strategy proposed in this paper.

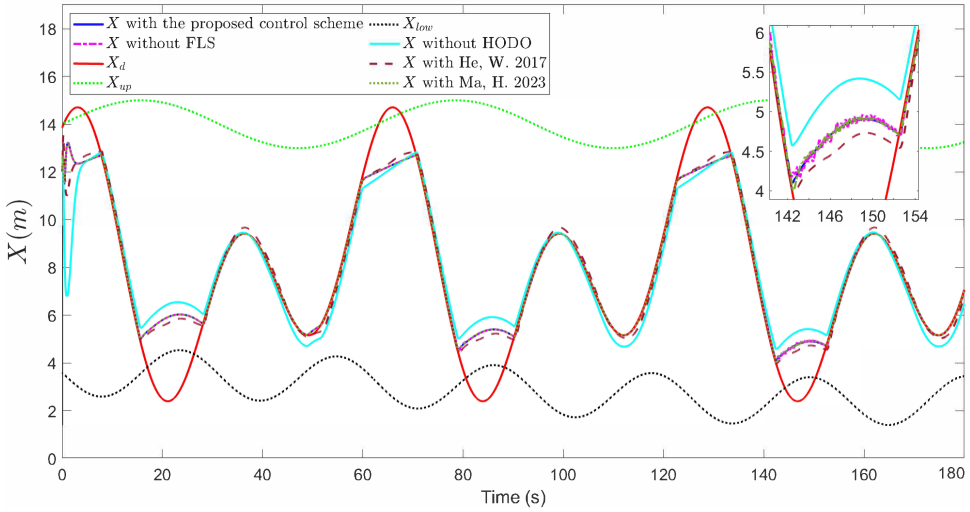

Figure 17. Tracking performance of X under different control schemes.

Table 3. The maximum error and convergence time of different methods in the X-axis.

Control Method	$\max_{t\in[0,\ 180]\mathrm{s}} \lvert X\ (\mathrm{m})\rvert$	Convergence Time (s)
proposed control scheme	12.5	2.5
without FLS	13	2.8
without HODO	16	–
proposed schene in [25]	8	10
proposed control scheme in [43]	13.2	2

It can be seen from the results presented in the above figures that the control scheme has good control performance for unmanned helicopters with system uncertainties, random disturbances and external disturbances.

6. Conclusions

An HODO-based adaptive safety fixed-time tracking control scheme is constructed for the uncertain UAH under random disturbances and external disturbances. In order to keep P and Ω constraints within the real-time security boundaries, the SPA is proposed, which can ensure the safety of the unmanned helicopter first when the system state conflicts with the security boundaries. The second-order DSC is utilized to ensure the desired safety signals are continuously differentiable. Then, the system uncertainties and the external disturbances are approximated by FLS and HODO. The Itô differential equation is utilized to solve the stochastic disturbances. Based on the fixed-time stability theory, the combination of the adaptive backstepping technique and Lyapunov stability theory, all signals of the unmanned helicopter are semi-globally fixed-time stable in probability. The compensation mechanism is utilized to weaken the impact of the filter error. In addition, the convergence time only depends on the devised parameters. Finally, the simulations prove the performance of the proposed control scheme. Therefore, the problem of parameter adjustment and optimization of fixed-time theory of unmanned helicopters under discrete time needs further study.

Author Contributions: Conceptualization, R.R., Z.W. and H.M.; methodology, R.R.; software, R.R. and Z.W.; validation, R.R., F.T. and B.J.; formal analysis, H.M.; writing—original draft preparation, F.T.; writing—review and editing, R.R. and Z.W.; supervision, B.J. and F.T. All authors have read and agreed to the published version of the manuscript.

Funding: This paper is supported in part by the National Natural Science Foundation of China under Grant (Grant Nos. 62301212, 62371182), the Program for Science and Technology Innovation Talents in the University of Henan Province (Grant No. 23HASTIT021), Major Science and Technology Projects of Longmen Laboratory (Grant No. 231100220300), Scientific and Technological Project of Henan Province (Grant Nos. 242102241063, 242102221025), the Key Scientific Research Projects of Universities in Henan Province (25A413001), and the Key Scientific Research Project of Henan University (24A590001) .

Data Availability Statement: The data presented in this study are available on request from the corresponding author. The data are not publicly available due to ownership reasons.

Conflicts of Interest: The authors declare no conflicts of interest.

References

1. De Assis, G.; Dos Santos, M.; Basilio, M. Use of the WASPAS method to select suitable helicoptersfor aerial activity carried out by the military police of the state of Rio de Janeiro. *Axioms* **2023**, *12*, 77. [CrossRef]
2. Vu, N.; Dang, D.; Dinh, T. Electric propulsion system sizing methodology for an agriculture multicopter. *Aerosp. Sci. Technol.* **2019**, *90*, 314–326. [CrossRef]
3. Caballero Morales, S.; Martinez Flores, J. Helicopter routing model with non-deterministic failure rate for evacuation of multiple oil platforms. *Comput. Ind. Eng.* **2020**, *139*, 105669. [CrossRef]
4. Yeo, H. Design and aeromechanics investigation of compound helicopters. *Aerosp. Sci. Technol.* **2019**, *88*, 158–173. [CrossRef]

5. Zhao, B.; Xian, B.; Zhang, Y.; Zhang, X. Nonlinear Robust adaptive tracking control of a quadrotor UAV via immersion and invariance methodology. *IEEE Trans. Ind. Electron.* **2015**, *62*, 2891–2902. [CrossRef]
6. Chen, F.; Jiang, R.; Zhang, K.; Jiang, B.; Tao, G. Robust backstepping sliding-mode control and observer-based fault estimation for a quadrotor UAV. *IEEE Trans. Ind. Electron.* **2016**, *63*, 5044–5056. [CrossRef]
7. Liu, H.; Yu, Y.; Zhong, Y. Robust trajectory tracking control for a laboratory helicopter. *Nonlinear Dyn.* **2014**, *77*, 621–634. [CrossRef]
8. Yang, S. Adaptive bounding-based dynamic inversion control of a coaxial compound helicopter. *IEEE Trans. Aerosp. Electron. Syst.* **2023**, *59*, 9451–9462. [CrossRef]
9. Raptics, I.; Valavanis, K.; Moreno, W. Anovel nonlinear backstepping controller design for helicopters using the rotation matrix. *Irrr Trans. Control. Syst. Technol.* **2011**, *19*, 465–473. [CrossRef]
10. Glida, H.; Abdou, L.; Chelihi, A.; Sentouh, C.; Hasseni, S. Optimal model-free backstepping control for a quadrotor helicopter. *Nonlinear Dyn.* **2020**, *100*, 3449–3468. [CrossRef]
11. Labbadi, M.; Cherkaoui, M. Robust adaptive backstepping fast terminal sliding mode controller for uncertain quadrotor UAV. *Aerosp. Sci. Technol.* **2019**, *93*, 105306. [CrossRef]
12. He, W.; Mu, X.; Zhang, L.; Zou, Y. Modeling and trajectory tracking control for flapping-wing micro aerial vehicles. *IEEE-Caa J. Autom. Sin.* **2021**, *8*, 148–156. [CrossRef]
13. Zhang, J.; Li, S.; Ahn, C.; Xiang, Z. Decentralized event-triggered adaptive fuzzy control for nonlinear switched large-scale systems with input delay via command-filtered backstepping. *IEEE Trans. Fuzzy Syst.* **2022**, *30*, 2118–2123. [CrossRef]
14. Xu, B.; Ma, Q.; Feng, J.; Zhang, J. Fault tolerant control of drone interceptors using command filtered backstepping and fault weighting dynamic control allocation. *Drones* **2023**, *7*, 106. [CrossRef]
15. Mullen, J.; Bailey, S.; Hoagg, J. Filtered dynamic inversion for altitude control of fixed-wing unmanned air vehicles. *Aerosp. Sci. Technol.* **2016**, *54*, 241–252. [CrossRef]
16. Omar, H. Designing anti-swing fuzzy controller for helicopter slung-load system near hover by particle swarms. *Aerosp. Sci. Technol.* **2013**, *29*, 223–234. [CrossRef]
17. Hu, Y.; Yang, Y.; Li, S.; Zhou, Y. Fuzzy controller design of micro-unmanned helicopter relying on improved genetic optimization algorithm. *Aerosp. Sci. Technol.* **2020**, *98*, 105685. [CrossRef]
18. Zhang, H.; Liu, J. Event-triggered fuzzy flight control of a two-degree-of-freedom helicopter system. *IEee Trans. Fuzzy Syst.* **2021**, *29*, 2949–2962. [CrossRef]
19. Cai, X.; Shi, K.; She, K.; Zhong, S.; Soh, Y.C.; Yu, Y. Performance error estimation and elastic integral event triggering mechanism design for T-S fuzzy networked control system under DoS attacks. *IEEE Trans. Fuzzy Syst.* **2023**, *31*, 1327–1339. [CrossRef]
20. Song, X.; Wu, C.; Song, S.; Stojanovic, V.; Tejado, I. Fuzzy wavelet neural adaptive finite-time self-triggered fault-tolerant control for a quadrotor unmanned aerial vehicle with scheduled performance. *Eng. Appl. Artif. Intell.* **2024**, *131*, 107832. [CrossRef]
21. Yu, Y.; Guo, J.; Chadli, M.; Xiang, Z. Distributed adaptive fuzzy formation control of uncertain multiple unmanned aerial vehicles with actuator faults and switching topologies. *IEEE Trans. Fuzzy Syst.* **2023**, *31*, 919–929. [CrossRef]
22. Fang, X.; Wu, A.; Shang, Y.; Dong, N. A novel sliding mode controller for small-scale unmanned helicopters with mismatched disturbances. *Nonlinear Dyn.* **2016**, *83*, 1053–1068. [CrossRef]
23. Wang, N.; Tao, F.; Fu, Z.; Song, S. Adaptive fuzzy control for a class of stochastic strict feedback high-order nonlinear systems with full-state constraints. *IEEE Trans. Syst. Man-Cybern.-Syst.* **2022**, *52*, 205–213. [CrossRef]
24. Chen, M.; Shi, P.; Lim, C. Adaptive neural fault-tolerant control of a 3-DOF model helicopter system. *IEEE Trans. Syst. Man-Cybern.-Syst.* **2016**, *46*, 260–270. [CrossRef]
25. He, W.; Yan, Z.; Sun, C.; Chen, Y. Adaptive neural network control of a flapping wing micro aerial vehicle with disturbance observer. *IEEE Trans. Cybern.* **2017**, *47*, 3452–3465. [CrossRef]
26. Wan, M.; Chen, M.; Yong, K. Adaptive tracking control for an unmanned autonomous helicopter using neural neural network and disturbance observer. *Neurocomputing* **2021**, *468*, 296–305. [CrossRef]
27. Li, M.; Wu, Z.; Deng, F.; Guo, B. Active disturbance rejection control to consensus of second-order stochastic multiagent systems. *IEEE Trans. Control. Netw. Syst.* **2023**, *10*, 993–1004. [CrossRef]
28. Kuznetsov, D. Development and application of the fourier method for the numerical solution of Ito stochastic differential equations. *Comput. Math. Math. Phys.* **2018**, *58*, 1058–1070. [CrossRef]
29. Chen, B.; Wu, C. Robust scheduling filter design for a class of nonlinear stochastic Poisson signal systems. *IEEE Trans. Signal Process.* **2015**, *63*, 6245–6257. [CrossRef]
30. Altan, A.; Hacioglu, R. Model predictive control of three-axis gimbal system mounted on UAV for real-time target tracking under external disturbances. *Mech. Syst. Signal Process.* **2020**, *138*, 106548. [CrossRef]
31. Hu, W.; Quan, J.; Ma, X.; Salah, M.; Shaker, A. Analytical design of optimal model predictive control and its application in small-scale helicopters. *Mathetatics* **2023**, *11*, 1845. [CrossRef]
32. Kalabic, U.; Li, N.; Vermillion, C.; Kolmanovsky, I. Peference governors for chance-constrained systems. *Automatica* **2019**, *109*, 108500. [CrossRef]
33. Borrelli, F.; Falcone, P.; Pekar, J.; Stewart, G. Reference governor for constrained piecewise affine systems. *J. Process. Control.* **2009**, *19*, 1229–1237. [CrossRef]
34. Yan, K.; Wu, Q. Adaptive tracking flight control for unmanned autonomous helicopter with full state constraints and actuator faults. *AeRospace Sci. Technol.* **2022**, *128*, 32–46. [CrossRef] [PubMed]

35. Dai, P.; Yan, B.; Han, T.; Liu, S. Barrier lyapunov function based model predictive control of a morphing waverider with input saturation and full-state constraints. *IEEE Trans. Aerosp. Electron. Syst.* **2023**, *59*, 3071–3081. [CrossRef]
36. Zhang, J.; Wang, Q.; Ding, W. Global output-feedback prescribed performance control of nonlinear systems with unknown virtual control coefficients. *IEEE Trans. Autom. Control.* **2022**, *67*, 6904–6911. [CrossRef]
37. Bu, X.; Jiang, B.; Lei, H. Nonfragile Quantitative prescribed performance control of waverider vehicles with actuator saturation. *IEEE Trans. Aerosp. Electron. Syst.* **2022**, *58*, 3538–3548. [CrossRef]
38. Verginis, C.; Bechlioulis, C.; Soldatos, A.; Tsipianitis, D. Robust trajectory tracking control for uncertain 3-DOF helicopter with prescribed performance. *IEEE-Asme Trans. Mechatronics* **2022**, *27*, 3559–3569. [CrossRef]
39. Ma, H.; Chen, M.; Feng, G.; Wu, Q. Adaptive fuzzy tracking control for unmanned autonomous helicopter with flight boundary constraints. *IEEE Trans. Fuzzy Syst.* **2023**, *31*, 184–198. [CrossRef]
40. Liu, X.; Liao, X. Fixed-time stabilization control for port-Hamiltonian systems. *Nonlinear Dyn.* **2019**, *96*, 1497–1509. [CrossRef]
41. Polyakov, A. Nonlinear feedback design for fixed-time stabilization of linear control systems. *IEEE Trans. Autom. Control.* **2011**, *57*, 2106–2110. [CrossRef]
42. Sun, Y.; Wang, F.; Liu, Z.; Zhang, Y.; Chen, C. Fixed-time fuzzy control for a class of nonlinear systems. *IEEE Trans. Cybern.* **2022**, *52*, 3880–3887. [CrossRef] [PubMed]
43. Ma, H.; Ren, R.; Tao, F.; Fu, Z.; Wang, N. FTDO-based adaptive fuzzy fixed-time tracking control for uncertain unmanned helicopter with output constraints. *Aerosp. Sci. Technol.* **2023**, *147*, 109019. [CrossRef]
44. Liu, S.; Niu, B.; Zong, G.; Zhao, X.; Xu, N. Adaptive fixed-time hierarchical sliding mode control for switched under-actuated systems with dead-zone constraints via event-triggered strategy. *Appl. Math. Comput.* **2022**, *435*, 127441. [CrossRef]
45. Liang, Y.; Li, Y.; Hou, Z. Adaptive fixed-time tracking control for stochastic pure-feedback nonlinear systems. *Int. J. Adapt. Control. Signal Process.* **2021**, *35*, 1712–1731. [CrossRef]